JOURNAL OF GEOPHYSICAL RESEARCH, VOL. ???, XXXX, DOI:10.1029/,

The solar-QBO interaction and its impact on stratospheric ozone in a zonally averaged photochemical-transport model of the middle atmosphere

J. P. McCormack and D. E. Siskind

Space Science Division, US Naval Research Laboratory, Washington DC, USA

L. L. Hood

Lunar and Planetary Laboratory, University of Arizona, Tucson AZ, USA

J. P. McCormack, Code 7646, Naval Research Laboratory, 4555 Overlook Avenue SW, Washington DC, 20375, USA. (john.mccormack@nrl.navy.mil)

Abstract. We investigate the solar cycle modulation of the quasi-biennial oscillation (QBO) in stratospheric zonal winds and its impact on stratospheric ozone with an updated version of the zonally averaged CHEM2D middle atmosphere model. We find that the duration of the westerly QBO phase at solar maximum is 3 months shorter than at solar minimum, a more robust result than in an earlier CHEM2D study due to reduced Rayleigh friction drag in the present version of the model. The modeled solar cycle ozone response, determined via multiple linear regression, is compared with observational estimates from the combined Solar Backscattered Ultraviolet (SBUV/2) data set for the period 1979–2003. We find that a model simulation including imposed solar UV variations, the zonal wind QBO, and an imposed 11-year variation in planetary wave 1 amplitude produces a lower stratospheric ozone response of ∼2.5% between 0°–20°S, and an upper stratospheric ozone response of ∼1% between 45–55 km, in good agreement with the SBUV-derived ozone response. This simulation also produces an (enhancement/reduction) in the (lower/upper) stratospheric temperature response at low latitudes compared to the effects of solar UV variations alone, which are consistent with model vertical velocity anomalies produced by the solar-modulated QBO and imposed changes in planetary wave forcing.

1. Introduction

A long-standing issue in understanding sun-climate connections is that both the magnitude and the altitude dependence of the apparent solar cycle variations in stratospheric ozone derived from satellite data sets differ markedly from estimates based on current models of stratospheric photochemistry [McCormack and Hood, 1996; Shindell et al., 1999; Hood, 2004]. Standard photochemical theory indicates that higher levels of ultraviolet (UV) irradiance during the maximum in the 11-year solar cycle increase the photolysis rate of molecular oxygen to produce more stratospheric ozone, and thus more radiative heating, in the upper stratosphere (35–50 km altitude) through ozone UV absorption. Photochemical model estimates of the low latitude ozone response to imposed changes in solar UV all generally peak at 2% near 35–40 km, and show variations of 1% or less both above and below this region [Hood, 2004; Soukharev and Hood, 2006]. In contrast, the 11-year ozone response derived from three different satellite-based data sets finds a different pattern in the altitude dependence of the ozone response at low latitudes [Soukharev and Hood, 2006]. This pattern consists of a positive response on the order of 2–4% (i.e., higher ozone at solar maximum) in the upper stratosphere between 40–45 km, a zero or weakly negative response in the middle stratosphere between 30–40 km, and a positive response of 2–4% in the lower stratosphere between 20–30 km.

Numerous modeling studies have shown that solar-induced changes in stratospheric ozone heating can produce changes in temperatures and winds that alter the upward propagation of planetary scale waves forced in the extratropical troposphere, ultimately producing a dynamical feedback that amplifies the original solar-induced effect and trans-

lates it to lower levels of the atmosphere [e.g., Haigh, 1996; Kodera et al., 1997; Rind, 2002; Kodera and Kuroda, 2002; Matthes et al., 2004, 2006]. Consistent with this hypothesis, global data sets of stratospheric ozone, temperature, and zonal wind exhibit quasi-decadal variability that is approximately in phase with the 11-year solar cycle [e.g. Labitzke and van Loon, 1988; Hood et al., 1993; Kuroda and Kodera, 2002; WMO, 2003; Hood, 2004; Crooks and Gray, 2005]. More recently, Austin et al. [2006] report that variations in sea surface temperatures may also contribute to the observed altitude dependence of the ozone response. The discrepancy between the predicted and observed ozone response to solar UV variability is a major source of uncertainty in our understanding of possible mechanisms linking solar variability and climate. The present study uses a zonally averaged (2D) photochemical-transport model of the middle atmosphere to identify possible dynamical origins of this discrepancy.

Currently, it is unclear how much of the observed altitude dependence in the ozone solar response is a true geophysical response to solar UV changes [e.g., Hood, 2004], and how much may be a statistical artifact arising from the relatively short length of existing global satellite data sets and the occurrence of large volcanic eruptions near periods of solar maximum [e.g., Lee and Smith, 2003]. Since stratospheric ozone photochemistry is relatively well understood, dynamical processes not included in most photochemical models are often cited as a possible geophysical origin for the observed vertical structure in the ozone response. Earlier studies have shown that the positive lower stratospheric ozone response is separate and distinct from volcanic effects [McCormack et al., 1997] and is consistent with a quasi-decadal modulation in the dynamics of the tropical lower stratosphere [Hood, 1997; Hood and Soukharev, 2003]. In the present study, we explore

the effects of solar-induced dynamical variations on lower stratospheric ozone with the zonally averaged CHEM2D photochemical-transport model.

Support for a solar influence on lower stratosphere dynamics is found in the observed 11-year variation of the quasi-biennial oscillation (QBO) in stratospheric equatorial zonal winds. A quasi-decadal modulation of the westerly QBO phase was first reported by Quiroz [1981] and later by Salby and Callaghan [2000] using an extended data record. An analysis of equatorial zonal winds by Hamilton [2002] confirms this result, but concludes that available data sets are still of insufficient length to unambiguously attribute this variability to changes in solar activity. Pascoe et al. [2005] report evidence of a solar cycle modulation of the mean descent rate of the easterly shear zone between 20–44 hPa in the ERA-40 data set, such that the easterly shear descends about 2 month faster during solar maximum. This is qualitatively consistent with the shorter westerly QBO phase during solar maximum reported by Salby and Callaghan [2000].

There also exists a complex relationship between the QBO and planetary wave activity in the wintertime extratropical stratosphere that may also be modified by the solar cycle. For example, breaking planetary waves in the wintertime stratosphere drive the mean meridional circulation in the middle atmosphere [Holton et al., 1995], and the propagation of these waves from the troposphere is sensitive to the phase of the zonal wind QBO [Baldwin et al., 2001]. In addition, the descent of the QBO easterlies is known to occur preferentially during the months of May–July, when the vertical component of the mean meridional circulation in the tropical lower stratosphere is weakest. A modeling study by Gray et al. [2004] suggests that equatorial upper stratospheric zonal wind anomalies related to both the solar cycle and the QBO can alter planetary wave propagation and

thus affect the frequency and timing of stratospheric sudden warmings in the Northern Hemisphere (NH) winter. The present study offers evidence that the combined effects of solar UV variations, the QBO, and planetary wave forcing could provide a possible explanation for the observed 11-year ozone response in the tropical lower stratosphere, where the ozone distribution is largely controlled by transport.

2D modeling studies are useful for evaluating the possible solar cycle modulation of the QBO, since the relative simplicity of the 2D model makes it straightforward to isolate internal and external sources of inter-annual variability over multi-decadal periods. Similar calculations with a 3D general circulation model (GCM) are much more computationally expensive, and the results are more difficult to interpret. For example, while a recent GCM study by Palmer and Gray [2005] using an internally generated zonal wind QBO found the QBO period to be 2 months shorter at solar maximum than at solar minimum, an unrealistically large change in solar irradiance was needed to produce a statistically significant response in the relatively short model integration (25 years).

The 2D modeling study of McCormack [2003], using an interactive representation of the zonal wind QBO, first showed that realistic changes in solar UV irradiance are capable of modulating the QBO period in a manner that was qualitatively consistent with the observed effect, i.e., a shorter duration of the QBO westerly phase during solar maximum. However, the difference in the duration of the modeled QBO westerly phase between solar minimum and solar maximum was only 1 month, whereas observations indicate a difference of 3–6 months [Salby and Callaghan, 2000].

The present study uses an updated version of the CHEM2D model used by McCormack [2003] to simulate the inter-annual variability in stratospheric ozone in response to

the 11-year solar cycle, the QBO, and quasi-decadal changes in the dynamical forcing of the stratospheric meridional circulation by planetary waves. This version of CHEM2D features a higher model top, increased vertical resolution, and an improved treatment of gravity wave drag in the middle atmosphere in which an imposed Rayleigh-type drag on the zonal winds now plays a lesser role [Siskind, 2003]. The goal of this study is to determine if the observed vertical structure in the 11-year ozone response can be explained by the interaction of the solar cycle, QBO, and planetary wave effects. We will focus in particular on the role of the QBO in producing the secondary maximum in the observed 11-year ozone response in the tropical lower stratosphere (i.e., 15–25 km altitude). Our results indicate that the improved model formulation produces a more robust solar cycle modulation of the zonal wind QBO compared to earlier results [McCormack, 2003]. We also find that the combined effects of solar UV variations, the zonal QBO, and planetary wave forcing can enhance the ozone response to changes in solar UV irradiance in both the lower and upper stratosphere in a manner that is qualitatively consistent with observations.

A description of the CHEM2D model is given in Section 2. Section 3 describes the analysis of model output using multiple linear regression. Section 4 presents results from a series of CHEM2D simulations including the effects of the 11-year solar cycle and the QBO. Section 5 discusses how these effects produce better agreement between the observed and modeled solar cycle variations in ozone. Section 6 contains a summary and outlines possible avenues of future research.

2. The CHEM2D Model

2.1. *Model description*

CHEM2D is a zonally averaged (2D) model that features a fully self-consistent treatment of radiative, photochemical, and dynamical processes of the middle atmosphere. [McCormack and Siskind, 2002; Siskind, 2003; McCormack et al., 2006]. The model photochemistry accounts for 54 different species, and now includes catalytic ozone loss due to bromine compounds. Model reaction rates are based on Sander et al. [2003]. The radiative and photochemical calculations are performed once per day, and the model dynamics are updated every 2 hours. The model extends from pole to pole with grid points spaced every 4.8° in latitude. The model vertical domain consists of 88 levels from the surface to pressure level $p = 6 \times 10^{-5}$ hPa ($\sim$116 km) that are spaced every 1.3 km. This version of the model offers twice the vertical resolution as earlier versions [McCormack and Siskind, 2002; McCormack, 2003].

The CHEM2D dynamical framework is based on the Transformed Eulerian Mean formulation, in which the residual meridional circulation is driven by zonally averaged sources of momentum and thermodynamic forcing [McCormack and Siskind, 2002]. The momentum sources include a parameterization for sub-grid scale gravity wave drag from both stationary and non-zero phase speed gravity waves, the Eliassen-Palm (EP) flux divergence associated with dissipating or breaking planetary waves, and parameterized vertical mixing of momentum by gravity wave breaking and molecular diffusion in the upper mesosphere. An altitude-dependent Rayleigh friction term is used to constrain the zonal wind field near the model top.

To simulate the zonal wind QBO, the CHEM2D model includes a parameterization of the upward momentum flux divergence associated with equatorial Kelvin and Rossby-gravity wave modes [Holton and Lindzen, 1972; Dunkerton, 1979; Gray and Pyle, 1989]. For a detailed description of the CHEM2D QBO parameterization, see McCormack and Siskind [2002]. This parameterization allows the period of the QBO to vary in response to changes in the strength of the model residual circulation. It has been used previously in the CHEM2D model to simulate QBO-related features in stratospheric constituent transport [McCormack and Siskind, 2002] and interactions between solar UV irradiance changes and the period of the zonal wind QBO [McCormack, 2003]. Figure 1a plots an altitude-time section of CHEM2D equatorial zonal winds illustrating the characteristics of the modeled QBO. The period of the QBO ranges from 24–33 months with an average period of 28 months, similar to observations.

One advantage of the CHEM2D model's interactive QBO parameterization is that, unlike models that employ a sinusoidal momentum source with a fixed period [e.g., Lee and Smith, 2003], it can capture possible solar-related photochemical-dynamical feedbacks that may influence the QBO. Models that produce a zonal wind QBO by relaxation to observed equatorial winds [e.g., Matthes et al., 2004] may capture the solar-QBO interaction, but they cannot isolate and quantify the origin of the interaction.

Another advantage of the CHEM2D model is that it is relatively inexpensive for performing long-term climate simulations. Recent GCM studies have been able to produce realistic QBO behavior in model zonal winds either by explicitly resolving equatorial wave modes with high vertical resolution [Giorgetta et al., 2006] or by adjusting the sub-grid scale gravity wave drag parameterization [Palmer and Gray, 2005]. To fully investigate

the impact of solar-QBO interactions on stratospheric ozone, these type of simulations should extend 50 years or longer and include fully coupled photochemistry, realistic solar UV forcing, and a realistic zonal wind QBO.

The CHEM2D gravity wave drag parameterization includes both stationary waves and non-stationary waves with discrete phase speeds ranging from -50 m/s to +50 m/s having a specified source distribution that varies with latitude [Siskind, 2003]. Additional non-stationary wave modes have been introduced in the tropics to produce a realistic semi-annual oscillation (SAO) in equatorial zonal wind throughout the middle atmosphere [McCormack, 2003]. Figure 1b compares the annual average CHEM2D zonal wind profile over the equator with a climatological wind profile based on observations from the Upper Atmosphere Research Satellite (UARS). In general, the CHEM2D zonal winds show good agreement with the UARS climatology, although there is an easterly bias in the CHEM2D equatorial zonal winds between 40–50 km altitude.

The increased model vertical resolution in the present version of CHEM2D was motivated in part by the study of McCormack [2003], which found a solar-cycle modulation of the zonal wind QBO period that was qualitatively consistent with, but smaller than, the quasi-decadal modulation reported by Salby and Callaghan [2000]. To improve the agreement between the observed and modeled solar-QBO effect, we have increased the model vertical resolution to obtain a better representation of parameterized sub-grid scale wave drag on the zonal winds. Results presented in Section 4.2 show that by decreasing the effect of Rayleigh friction on zonal winds near the stratopause, the present high-vertical resolution CHEM2D model produces a more robust solar cycle modulation of the QBO period compared to the earlier result of [McCormack, 2003].

CHEM2D solar UV variations over the 11-year cycle are specified as a function of wavelength from 125–300 nm using the satellite-based estimates of Lean et al [1997]. These variations are imposed as a sinusoidal 11-year variation. Unlike earlier studies that have performed steady state calculations under both solar maximum and solar minimum conditions, this time-varying approach allows us to evaluate the solar response through multiple realizations of the QBO and annual cycle. This is important since the phase relationship between the QBO and annual cycle changes over time, which can introduce an internal beat period in model transport fields on decadal time scales [e.g., McCormack and Siskind, 2002, their Fig. 11]. Furthermore, a recent 3D modeling study by Austin et al. [2006] demonstrates that using time-varying solar forcing produces a stratospheric ozone response that is in better agreement with observations than using fixed solar forcing for maximum and minimum conditions separately, even when the effects of the QBO are not considered.

2.2. *Experimental setup*

Table 1 lists a series of CHEM2D model experiments that are designed to further examine the solar cycle modulation of the zonal wind QBO reported by McCormack [2003] and to assess the combined effects of solar UV variations, the QBO, and planetary wave activity on the 11-year response in stratospheric ozone and temperature. All model simulations are 50 years in length unless otherwise noted.

We begin with a control experiment (EXP0 in Table 1) that includes the interactive QBO parameterization with fixed solar UV irradiance. In the first experiment with varying solar UV (EXP1), we impose an 11-year sinusoidal variation in solar UV irradiance based on estimates from Lean et al [1997]. The zonal wind QBO parameterization is not

included in EXP1 in order to produce a "pure" solar signal in the model ozone fields. An additional simulation without the QBO (EXP1RF) uses the Rayleigh friction drag profile of McCormack [2003] to demonstrate how it affects the model's dynamical response to solar UV variations in the upper stratosphere (see section 4.1).

Experiment 2 (EXP2) is an extended 150-year simulation that includes both the 11-year solar UV variations and the zonal wind QBO parameterization. With the longer simulation, we are able to obtain a statistically significant solar cycle modulation of the QBO (see Section 4.2). Experiment 3 (EXP3) introduces an 11-year modulation in the extratropical planetary wave forcing, which is consistent with the observational estimates of Hood and Soukharev [2003], in addition to the solar UV and QBO effects. Finally, the fourth experiment (EXP4) includes the solar UV and planetary wave forcing effects but no zonal wind QBO parameterization. A comparison of results from EXP3 and EXP4 shows that the imposed 11-year variations in solar UV and planetary wave amplitudes produce a larger quasi-decadal signal in lower stratospheric ozone when the zonal wind QBO is present.

3. Linear regression model

This section describes the multiple regression statistical model used to analyze the results from the experiments listed in Table 1. Multiple linear regression models have long been a standard tool for estimating trends in stratospheric ozone [e.g. WMO, 1991; SPARC, 1998, and references therein]. The standard approach is to assume that the temporal behavior of a zonally averaged time series (i.e., ozone or temperature) can be approximated by a least-squares fit to a linear model with trend, QBO, and 11-year solar cycle components. Initially, the motivation for this approach was to ensure that natural

sources of inter-annual variability did not project onto estimates of the anthropogenic trends in ozone. With the advent of longer satellite-based data sets, it became feasible to apply this model to quantify the effects of the QBO and the solar cycle on stratospheric ozone and temperature in order to facilitate model-data comparisons of inter-annual variability [Hood and McCormack, 1992; Randel and Cobb, 1994; McCormack and Hood, 1996; Crooks and Gray, 2005; Soukharev and Hood, 2006].

Here we adopt an approach similar to that of Lee and Smith [2003] where we apply a multiple linear regression model to output from a 2D model in order to isolate the 11-year variability in ozone and temperature. The regression model quantifies the components of interannual variability in the dependent time series (i.e., the model output) associated with a set of independent explanatory time series (i.e., the 11-year solar UV forcing and the QBO). Using this approach, we are able to make direct comparisons between the modeled solar cycle variability in ozone and the SBUV(/2)-derived estimates of the 11-year ozone response of Soukharev and Hood [2006].

One difference between our regression model and that of Soukharev and Hood [2006] is the absence of a trend term and the accompanying auto-correlation term. Aside from the solar UV and QBO effects described above, no interannual variability or trends are directly imposed on the model's photochemical constituents, therefore there is no need to model this trend statistically. Regression analyses of CHEM2D model ozone output conducted both with and without the trend and autocorrelation terms show negligible differences in the resulting estimates of the solar cycle response. Therefore, we elect not to include this term in our analysis.

Previous observational studies have described the QBO in their regression models using either a lagged time series of the zonal wind QBO at one particular level [McCormack and Hood, 1996; Soukharev and Hood, 2006], a combination of zonal wind time series at two different levels where the time variability is in approximate quadrature [Brunner et al., 2006], or proxy time series based on the set of linear orthogonal basis functions determined from a principal component or empirical orthogonal function analysis of equatorial stratospheric zonal winds [e.g., Randel and Wu, 1996; Crooks and Gray, 2005]. We have tested each form of QBO representation in our regression model and found no significant differences in the derived solar regression coefficients. We note that the CHEM2D model's representation of the zonal wind QBO is only an approximation of the true zonal wind QBO, and as such may not capture all the temporal variability in the observed QBO. Recent 2D photochemical modeling studies have shown that a lagged QBO proxy time series may introduce artifacts in solar regression coefficients if the QBO period is highly irregular over the course of several decades (A. Smith, personal communication, 2006). To avoid this possibility, our regression model employs a QBO proxy time series based on the results of a principal component analysis of CHEM2D equatorial zonal winds.

The multiple linear regression model used in the present study is of the form

$$y(t) = \mu_i(t) + \gamma_S X_S(t) + \gamma_{QBO1} X_{QBO1} + \gamma_{QBO2} X_{QBO2}. \quad (1)$$

Here y is the model time series (i.e., zonal mean ozone or temperature), μ_i is the corresponding long-term mean value for each month $i = 1, \ldots, 12$, and X_S is a 11-year sinusoidal variation in solar UV (see Fig. 2, top curve). X_{QBO1} and X_{QBO2} are time series representing the two leading principal components derived from a linear system of model equatorial zonal winds between 10–70 hPa from each experiment. The ozone

(temperature) regression coefficients γ_S, γ_{QBO1}, and γ_{QBO2} are calculated in terms of volume mixing ratio (Kelvin) on a constant pressure (p) grid and converted to altitude (z) using the relation $z = -H\log(p/1013)$, where the pressure scale height H is taken to be a constant 7.021 km. The seasonal dependence of each regression coefficient is represented by a series of harmonic functions [Randel and Cobb, 1994]. Uncertainties in the regression coefficients are determined from the error covariances of the least-squares fit. Where appropriate, $\pm 2\sigma$ values of a regression coefficient's uncertainties are quoted in parentheses.

To illustrate the QBO proxy time series, Figure 2 plots the normalized time series of X_{QBO1} and X_{QBO2} from the control run (EXP0). Together they explain over 90% of the temporal variance in the model equatorial zonal winds between 10–70 hPa. Figure 3 shows the latitude and altitude dependences of the ozone regression coefficients γ_{QBO1} and γ_{QBO2} calculated from regression analysis of the CHEM2D ozone fields from the EXP0 run; shaded regions are not statistically significant at the 2σ level. For each experiment, the QBO proxy time series are determined by principal component analysis of output zonal wind fields prior to the regression analysis.

The regression model (1) is applied to the CHEM2D model ozone and temperature fields from each of the experiments listed in Table 1, which are diurnally averaged and output on the first day of each calendar month. All regression analyses are based on 50 years of model output to facilitate comparison of regression coefficients' statistical significance among the different experiments.

4. Results

Here we present results from the CHEM2D model experiments that are described in Section 2.2 and summarized in Table 1.

4.1. Experiment 1: Varying solar UV only

Figure 4 plots the annual average solar regression coefficients derived from the EXP1 ozone fields between 18–65 km, which are expressed in terms of the percentage change in ozone from solar minimum to maximum. Consistent with earlier modeling studies [Hood, 2004], we find the largest positive ozone response (∼3%) between 35–40 km, in contrast to the observational results that find the largest response in the upper stratosphere. Shaded regions in Fig. 4 denote where the solar regression coefficients from this 50-year run are not different from zero at the 2σ level. Typical 2σ uncertainty values from the analysis of EXP1 are 0.1% or less. As Fig. 4 indicates, the EXP1 regression coefficients are statistically significant throughout most of the stratosphere and lower mesosphere.

Next, we compare the modeled stratospheric ozone response with observational estimates derived from the combined 24-year (1979–2003) Solar Backscatter Ultraviolet (SBUV) and SBUV2 ozone profile data set by Soukharev and Hood [2006] using a similar multiple linear regression model. Figure 5 plots the annual average SBUV(/2) solar regression coefficients as a function of latitude and approximate altitude. Since SBUV profile measurements are limited to sunlit regions, solar regression coefficients are only computed for the latitude region from 60°S–60°N. Typical values of the 2σ uncertainties in the SBUV-derived solar regression coefficients are ±1% throughout most of the stratosphere.

As mentioned in the Introduction, the altitude and latitude dependences of the modeled solar response in stratospheric ozone from EXP1 in Figure 4 show marked disagreement with the SBUV(/2)-derived response in Figure 5. Most noticeably, the modeled ozone response in the tropics peaks near 35 km, whereas the SBUV(/2) solar coefficients in the tropics peak between 45–50 km. Furthermore, SBUV(/2) data show no statistically significant ozone response over the solar cycle in the tropics from 30–45 km. Two regions with somewhat reasonable agreement are found near 35 km between 40°–50°S and 50°–60°N latitude, where the EXP1 results indicate a 2–3% ozone increase from solar minimum to solar maximum. In the lower stratosphere (18–25 km), the EXP1 results show little to no significant ozone response throughout the tropics, whereas the SBUV(/2) results indicate a secondary subtropical maximum in the ozone response with peak values of 2.5–3% at the lowest analyzed level at 50 hPa (∼21 km).

Currently, it is not clear why the observed upper stratospheric ozone response exceeds photochemical model estimates. Langematz et al. [2005] proposed that this feature could be a response to solar-modulated production and transport of mesospheric odd nitrogen to the tropical stratopause region. However, an analysis of HALOE NO_x records over the last solar cycle by Hood and Soukharev [2006] shows no significant 11-year variation in the upper stratosphere to support this assertion. As shown in section 4.3, model simulations that include imposed variations in planetary wave forcing (EXP3 and EXP4) produce a somewhat larger upper stratospheric ozone response than solar forcing alone (EXP1), in better agreement with the observed upper stratospheric ozone response (Fig. 5).

The lack of a significant observed ozone response in the middle stratosphere (i.e., 30–40 km altitude) could not be reproduced in EXP1. Lee and Smith [2003] have suggested

that the zero or slightly negative mid-stratospheric ozone response seen in the observations is due to the effects of major volcanic eruptions that occurred near the maximum of solar cycles 21 and 22. Their assertion was based on a zonally averaged (2D) photochemical model simulation in which the anomalous heating due to volcanic eruptions produces a quasi-decadal variation of ∼50% in the strength of the westerly zonal wind QBO phase, contrary to observations. Since the CHEM2D model does not include heterogeneous chemical reactions on stratospheric aerosols, we cannot test this claim directly. We note that an inter-comparison of the observed 11-year ozone response in SBUV(/2), HALOE, and SAGEI/II data by Soukharev and Hood [2006] finds a minimum in the stratospheric ozone response near 35 km in all three data sets regardless of whether or not periods of high volcanic aerosol loading were included in the analyses.

One major difference between the high-vertical resolution model used in the present study and the lower-vertical resolution model used in McCormack [2003] is in the magnitude of the prescribed Rayleigh friction term used to constrain the zonal winds in the mesosphere. With the higher model top and increased vertical resolution, it is no longer necessary to use such a strong damping factor on mesospheric winds. Figure 6(a) compares the Rayleigh friction profile used in McCormack [2003] (gray curve) with the profile used in the present study (black curve). The old Rayleigh friction profile makes a non-zero contribution to the momentum budget near the stratopause, where the solar-induced heating anomalies are largest. In contrast, the effects of the new Rayleigh friction profile are limited to the upper portion of the mesosphere.

The consequences of the reduced Rayleigh friction profile on the solar-induced zonal wind anomalies near the stratopause can be seen in Figure 6b, which compares the solar

cycle response in equatorial zonal winds at 50 km from EXP1 with the zonal wind response from an identical model run using the original Rayleigh friction profile of McCormack [2003], denoted as EXP1RF in Table 1. The 11-year variation in the EXP1 zonal wind anomalies (computed by subtracting the long term monthly mean) is much larger than in the EXP1RF run, and compares favorably with estimates of the solar cycle variability in equatorial zonal wind from meteorological analyses [Crooks and Gray, 2005]. This result demonstrates that the increased Rayleigh friction in the earlier CHEM2D study of McCormack [2003] limited the model's upper stratospheric dynamical response to solar UV variations. The implications of this result for modeling the solar cycle modulation of the QBO period are discussed further in Section 4.2.

In summary, the EXP1 modeled ozone response due solely to changes in solar UV irradiance does not reproduce the observed vertical structure in the 11-year ozone response in the stratosphere at low latitudes. In the following sections, we present results from additional CHEM2D experiments that include the effects of the zonal wind QBO and decadal variability in planetary wave forcing. These results show that interactions between solar UV changes, the QBO, and planetary wave forcing can improve the agreement between the modeled and observed 11-year variation in stratospheric ozone.

4.2. Experiment 2: Solar UV and QBO effects

This section presents results from a 150-year CHEM2D simulation that includes both solar UV and QBO effects (EXP2). This simulation demonstrates the solar cycle modulation of the zonal wind QBO and its impact on stratospheric ozone and temperature. The methodology of EXP2 is similar to an earlier study by McCormack [2003] that used a version of CHEM2D with a 2.6 km vertical grid spacing and a model top near ∼106 km.

This study found a small (∼1 month) decrease in the length of the QBO westerly phase during solar maximum that was qualitatively similar to, but much smaller than, the 3–6 month decrease in the QBO westerly phase duration at solar maximum reported by Salby and Callaghan [2000]. The present version of CHEM2D produces a larger solar cycle modulation of the QBO westerly phase than that reported by McCormack [2003].

Figure 7 compares time series of zonal winds over the equator at the 32 hPa level (∼26 km) from years 1-51 of the EXP2 (i.e., varying solar UV, gray curve) and EXP0 (i.e., fixed solar UV, black curve) experiments. Both simulations are initialized with the same model constituent and transport fields, and they both begin with the same UV irradiance values corresponding to solar maximum. We find that the two time series start to differ by year 6, corresponding to solar minimum in EXP2, and remain out of phase throughout this period owing to differences in the length of the QBO westerly phase between solar maximum and solar minimum in EXP2. This behavior is in better agreement with the observed solar cycle modulation of the QBO than the earlier results of McCormack [2003] that produced a weaker solar cycle modulation of the QBO westerly phase.

To quantify the solar cycle modulation of the model zonal wind QBO, we have calculated the lengths of the the individual easterly and westerly QBO phases at 32 hPa in EXP2 occurring within a 20-month window centered on solar maximum and minimum. Figure 8 plots the duration of the individual easterly and westerly QBO phases at 32 hPa from the entire 150 years of EXP2 output for solar minimum and solar maximum conditions. We find that the average westerly QBO phase at 32 hPa is 15 months at solar maximum and 18 months at solar minimum. A Student's t–test shows that this 3 month difference is statistically significant at the 98% confidence level. This result is in better agreement

with the observed 3-6 month difference reported by Salby and Callaghan [2000] than the 1-month difference reported earlier by McCormack [2003].

The proposed origin of the modeled solar cycle modulation of the westerly QBO phase, which has been described previously by McCormack [2003], is summarized here. Increased heating at solar maximum in the upper stratosphere produces stronger upward vertical motion near the summer subtropical latitudes and stronger meridional flow across the equator from the summer to winter hemisphere. The anomalous advection of easterly momentum from the summer hemisphere by the meridional component of the residual circulation offsets the westerly zonal wind tendencies produced by the parameterized gravity wave drag that drives the SAO westerly phase. This reduces the westerly zonal wind tendency to give overall weaker westerly flow in the equatorial upper stratosphere during solar maximum [see Fig. 6 and McCormack, 2003, Fig.5]

Since the model QBO westerlies tend to emerge during the SAO westerly phase, solar-induced changes in the strength of the upper stratospheric westerly flow will affect the timing and duration of the QBO westerly phase. The model results indicate that the weaker westerly zonal wind tendencies under solar maximum conditions favor a more rapid transition to the QBO easterly phase, and thus a shorter QBO west phase. In contrast, the timing and duration of the modeled QBO easterly phase is affected primarily by the annual cycle in tropical upwelling in the lower stratosphere. This is also seen observationally in the preferential "stalling" of the QBO easterly phase during NH winter. As a result, the modeled dynamical response to varying solar UV in the tropical upper stratosphere affects the duration of the QBO west phase more than it affects the QBO east phase.

Fig. 7 and Fig. 8 illustrate the solar cycle modulation of the westerly QBO phase. The high-vertical resolution version of CHEM2D employed in the present study produces a larger average difference in the length of the QBO west phase (3 months) between solar maximum and minimum than was originally found by McCormack [2003] (1 month). The larger effect is a consequence of the reduced Rayleigh friction term in the present version of CHEM2D, which produces a larger solar cycle variation in model dynamics near the stratopause (Fig. 6b) as compared to the earlier low-vertical resolution version of the model.

McCormack [2003] found that the solar cycle modulation of the QBO produces a quasi-decadal variation in lower stratospheric tropical upwelling. This variation can affect both ozone and temperature in the tropical lower stratosphere, where transport effects generally dominate over photochemical and radiative effects. The effect of the solar-QBO interaction on ozone can be seen in Figure 9, which plots the annual average ozone solar regression coefficients derived from the first 50 years of EXP2. The presence of the QBO increases the model's interannual variability, and so the resulting 2σ uncertainty estimates in the regression coefficients are larger than in EXP1. Typical values of the 2σ uncertainty estimates for the EXP2 ozone regression coefficients range from 0.2% in the upper stratosphere to 0.5% in the lower stratosphere. As with the EXP1 results, we find a statistically significant ozone response throughout much of the stratosphere and lower mesosphere in the EXP2 results.

Comparing the ozone regression coefficients derived from EXP1 (Fig. 4) and from the first 50 years of EXP2 (Fig. 9), we find that the 11-year ozone response in the tropical lower stratosphere increases when the effects of the zonal wind QBO are included.

The largest change is seen between 0–10°S latitude and 20–25 km altitude, where the peak ozone response increases from (1.5±0.03)% in EXP1 to (2.2 ±0.4)% in EXP2. The fact that this enhancement is not centered over the equator is likely a consequence of a meridional asymmetry in the modeled zonal wind QBO produced with the higher-vertical resolution version of CHEM2D. For example, the peak zonal wind QBO amplitude in EXP2 is centered near 10°S, whereas an earlier version of CHEM2D produced a zonal wind QBO centered over the equator [see, e.g., McCormack and Siskind, 2002, Fig. 4] that is more consistent with the observed latitude structure of the QBO [Baldwin et al., 2001; Salby and Callaghan, 2006].

The effect of the solar-QBO interaction on temperature can be seen in Figure 10, which plots the annual average temperature regression coefficients derived from the first 50 years of EXP2. The EXP2 temperature response is statistically significant at the 2σ level throughout most of the stratosphere and lower mesosphere, and exhibits a local maximum in the tropical lower stratosphere, similar to the modeled ozone response in Figure 9. The peak lower stratospheric temperature response in EXP2 of (0.6±0.06) K near 10°S is significantly larger than the corresponding temperature response of (0.3±0.01) in EXP1 (not shown).

The presence of the equatorial zonal wind QBO also modifies the modeled solar cycle variation in extratropical dynamics. For example, Figure 11 compares the composite zonal wind differences (i.e., solar maximum minus solar minimum) over the Northern Hemisphere (NH) extratropics in winter computed from EXP1 (Fig. 11a), and EXP2 (Fig. 11b-d). The composites in Fig. 11a and Fig. 11b are constructed from 50 years of model output within ±1 year of solar maximum or minimum, giving a total of 12 members

in each category. Regions of statistically significant differences are determined using the Student's t–test. In the case of EXP1, where only solar UV effects are included, Fig. 11a shows negligible zonal wind differences on Dec. 1 (top panel). By Jan. 1 (middle panel) a 2–4 ms^{-1} increase in westerly flow at solar maximum develops in the midlatitude upper stratosphere and lower mesosphere, which propagates poleward and downward by Feb. 1 (bottom panel).

Similar behavior is noted in the EXP2 zonal wind fields (Fig. 11b), although now the presence of the zonal wind QBO introduces a higher degree of interannual variability that reduces the statistical significance of the differences. Figure 11b shows that the QBO produces larger extratropical zonal wind anomalies in NH winter than in the case with no QBO (EXP0, Fig. 11a). The general pattern of positive upper stratospheric zonal wind anomalies at solar maximum appearing in early Northern winter and propagating poleward and downward in the following months is similar to the observed zonal wind response [Kuroda and Kodera, 2002; Matthes et al., 2004].

To further investigate the combined solar cycle-QBO effect on the zonal winds, we sort the composite zonal wind differences from EXP2 according to the sign of the model zonal wind over the equator at 32 hPa ($\sim$26 km), using the model output from the month closest to solar maximum/minimum with the appropriate QBO phase. This produces a subset of 4 years for each case. We find a more robust extratropical zonal wind response during Northern winter in QBO east years (Fig. 11c) than in QBO west years (Fig. 11d).

An examination of zonal wind anomalies and Eliassen-Palm flux calculations from EXP0 (i.e., QBO with no solar effect, not shown) indicates that the wintertime NH stratosphere exhibits reduced equatorward propagation of planetary wave activity during easterly QBO

phase [e.g. Holton and Tan, 1980]. This change in planetary wave propagation produces greater drag on the zonal winds poleward of 60°N and a reduction in the planetary wave drag on the zonal winds at midlatitudes. In this way, the model zonal wind anomalies tend to reinforce the "pure" zonal wind response to the 11-year solar UV variations (Fig. 11a) during QBO east years, and tend to oppose the pure solar response during QBO west years. This behavior is qualitatively consistent with earlier observational studies that found a significant correlation between solar activity and stratospheric temperatures or geopotential heights in Northern winter in years when the equatorial zonal wind QBO was in its easterly phase [Labitzke and van Loon, 1988; Labitzke, 2005].

4.3. Experiments 3 and 4: Effects of imposed planetary wave forcing

Observational and 3D modeling studies indicate that the combined effects of the solar cycle and the QBO on stratospheric winds in the Northern winter extratropics can reduce planetary wave activity at solar maximum and alter the mean meridional circulation of the middle atmosphere [Hood and Soukharev, 2003; Matthes et al., 2004; Gray et al., 2004; Palmer and Gray, 2005]. Since planetary wave activity drives the upward component of the mean meridional circulation in the tropical stratosphere [Holton et al., 1995], it has been suggested that a decadal modulation in planetary wave activity associated with solar activity could contribute to the observed 11-year signal in lower stratospheric ozone seen in Figure 5 [Hood, 2004]. The key to this proposed mechanism is understanding the nonlinear interaction between the QBO, planetary waves, and the mean meridional circulation [Salby and Callaghan, 2006].

Unlike 3D models where the tropospheric planetary wave forcing can vary in response to changes in the background zonal winds, CHEM2D employs fixed planetary wave 1

amplitude at the model lower boundary (1.3 km). Consequently, the results of EXP1 and EXP2 could be missing a feedback effect where changes in planetary wave forcing in response to solar-induced zonal wind anomalies (e.g., Fig. 11) alter tropical upwelling and ultimately produce an enhanced dynamical response in ozone and temperature in the tropical lower stratosphere. To evaluate this effect, we have performed a third experiment (EXP3) where, in addition to the 11-year solar UV variation and the QBO, we impose an 11-year variation in planetary wave 1 amplitude at the model lower boundary.

The amplitude of the imposed planetary wave forcing is based on the study of Hood and Soukharev [2003], who found evidence of a quasi-decadal variation in NH eddy heat flux of $\sim$10% that was anti-correlated with the 11-year solar cycle. Hood and Soukharev [2003] also found indications of a similar, albeit smaller, quasi-decadal variation in the Southern Hemisphere (SH) eddy heat flux; this result is considered to be less reliable than the NH eddy heat flux variation because of the poor data coverage at high southern latitudes.

These variations in eddy heat flux may be an indirect response of the tropospheric circulation to the 11-year solar cycle, as has been suggested, or they may be the result of internal dynamical variability unrelated to the solar cycle. In either case, the goal of this experiment is to quantify the combined effect of the solar UV, QBO, and planetary wave variations on stratospheric ozone and temperature within the 2D modeling framework. The results of this experiment provide further insight into the possible origin of the observed altitude dependence of the 11-year ozone response and can provide guidance for more detailed 3D model experiments in the future.

Figure 12a plots planetary wave 1 amplitudes used in the CHEM2D model as a function of latitude. In EXP3, we impose a 10% variation in the wave 1 amplitude over the winter

season in both hemispheres such that the wave forcing is higher during solar minimum and lower during solar maximum. (Note: CHEM2D experiments with fixed planetary wave 1 amplitude use the solar minimum values in Fig. 12a). Although the SH eddy heat flux variations reported by Hood and Soukharev [2003] may be less reliable than the NH estimates, we apply the wave 1 amplitude to both hemispheres to establish a theoretical upper limit on the resulting ozone and temperature variability.

To demonstrate that the imposed 10% variation in planetary wave 1 amplitude is consistent with the decadal variations in NH eddy heat flux reported by Hood and Soukharev [2003], Figure 12b plots a time series of the NH average vertical component of the EP flux (F_z) at 100 hPa for January from Experiment 3. The eddy heat flux is proportional to F_z [Andrews et al., 1987], and both are commonly used to diagnose the strength of the planetary wave forcing on the stratospheric mean meridional circulation. The imposed 11-year variation in planetary wave 1 amplitude produces a $\sim$10% variation in F_z in NH winter, with stronger forcing at solar minimum and weaker forcing at solar maximum. This time dependence agrees qualitatively with the 3D modeling study of Matthes et al. [2004] that reported a weaker meridional circulation at solar maximum in Northern winter.

Figure 13 plots the annual average solar regression coefficients for ozone from EXP3. Overall, the latitude and altitude dependences of the EXP3 regression coefficients are similar to the EXP2 results, with a peak ozone response between 35–40 km and a secondary maximum in the lower stratosphere centered at 10°S. However, the addition of the planetary wave 1 forcing in EXP3 produces a larger peak ozone response in the tropical lower stratosphere of (2.6$\pm$0.5)% than seen in the EXP2 results (Fig. 9). The larger EXP3 ozone response in the tropical lower stratosphere is accompanied by a small region

of reduced response (1.5±0.4%) at 30 km. We also note a slightly larger ozone response in the equatorial upper stratosphere. Although the differences between the lower stratospheric ozone responses in EXP2 and EXP3 are not statistically significant, the imposed planetary wave forcing in EXP3 produces better qualitative agreement with the observed lower stratospheric ozone response. The imposed planetary wave forcing also produces statistically significant ozone responses of 2–3% in the NH between 40°N–70°N peaking near 18 km and in the Southern Hemisphere poleward of 80°S between 20–30 km.

Figure 14 plots the solar regression coefficients derived from the CHEM2D model temperatures for EXP3. As in the case of EXP2, we find that the enhanced lower stratospheric ozone response in EXP3 (Fig. 13) near 10°S is accompanied by an enhanced lower stratospheric temperature response of (0.7±0.4) K. Near the equatorial stratopause, we find that the EXP3 temperature response is somewhat diminished compared to the EXP2 result (Fig. 10). Most differences in the temperature response between EXP2 and EXP3 are not statistically significant from each other below 50 km. However, the EXP3 results in Fig. 14 do show large positive temperature responses of ∼1.6 K at high latitudes in both hemispheres between 50–60 km that are significantly larger than the corresponding EXP2 temperature response.

The larger modeled ozone and temperature responses in the lower stratosphere in EXP3 suggest that the combined effects of planetary wave forcing and solar/QBO effect in EXP3 could help explain the observed 2-3% quasi-decadal variability in lower stratospheric ozone reported by Soukharev and Hood [2006]. To determine the model's response to the imposed planetary wave variability in the absence of the QBO, a fourth 50-year simulation

(EXP4) was carried out where only the solar UV and planetary wave amplitude variations were included.

Figure 15 plots the solar ozone regression coefficients for EXP4. We find that a peak lower stratospheric ozone response in EXP4 of (2.2±0.4)% that is generally less than the peak response in EXP3, which includes the effects of the QBO. Although these differences are not statistically significant at the 2σ level due to the relatively large amount of interannual variability in the model ozone fields, we find that including the QBO in EXP3 produces better agreement with the observed lower stratospheric ozone response.

Interestingly, the equatorial upper stratospheric ozone response in EXP4 is slightly larger than in EXP3, in better agreement with the observed upper stratospheric ozone response. Regression analysis of the EXP4 temperatures (Figure 16) finds that, in the absence of the QBO, the 11-year planetary wave forcing produces a smaller upper stratospheric temperature response at low latitudes and a larger upper stratospheric temperature response at high latitudes as compared to EXP3. Regression analysis of both the EXP3 and EXP4 temperatures for December-January-February and June-July-August periods (not shown) indicates that these high-latitude upper stratospheric temperature responses are largest in the winter hemispheres, similar to the seasonal dependence found in earlier analyses [McCormack and Hood, 1996; Hood, 2004].

Both the EXP3 and EXP4 temperature responses suggest that the imposed variation in planetary wave 1 amplitude modulates the residual circulation in the upper stratosphere, producing more upwelling at low latitudes and more downwelling at high latitudes during solar maximum. This effect is more pronounced in EXP4, since the presence of the QBO in EXP3 introduces residual circulation anomalies of alternating sign that act to

reduce the overall effect of the planetary wave variations in the annual mean response. The diminished equatorial upper stratospheric temperature response in EXP4 has consequences for ozone in the upper stratosphere, as we discuss further in Section 5. In the tropical lower stratosphere, however, EXP4 produces a smaller temperature response than in EXP3, indicating the importance of the the QBO's contribution to the quasi-decadal dynamical variability in this region.

To illustrate this point, Figure 17 plots composite annual mean differences (solar maximum minus solar minimum) in model vertical velocity ($\bar{w}^*$) from EXP1, EXP2, EXP3, and EXP4. Overall, the effects of the planetary wave forcing in EXP4 produce the strongest upwelling in the tropical upper stratosphere (above 45 km) at solar maximum, and the strongest downwelling in the extratropical upper stratosphere. Only simulations that include the QBO, however, exhibit much of a solar cycle variation in the lower stratosphere (below 35 km). Although statistically significant differences cannot be obtained due to the larger interannual variability associated with the QBO, the $\bar{w}^*$ anomalies in EXP2 and EXP3 suggest a decrease in tropical upwelling at solar maximum (i.e., negative anomaly in $\bar{w}^*$) between 0°–20°S near 25 km. An examination of the seasonal variation in the $\bar{w}^*$ anomalies (not shown) finds the strongest downwelling at high latitudes in winter, which is consistent with the seasonal dependence of the high latitude temperature response found in the upper stratosphere in both EXP3 and EXP4.

The following section examines the altitude dependence of the modeled 11-year ozone response in more detail. We find that changes in the residual vertical velocity produced by the combined effects of solar UV variation, the QBO, and quasi-decadal variability in

planetary wave forcing can in turn produce vertical structure in the 11-year stratospheric ozone response similar to that seen in the SBUV(/2) record over the 1979–2003 period.

5. Comparison with SBUV(/2) ozone response

As the model results in Section 4 show, incorporating the effects of the zonal wind QBO (EXP2) and an additional 11-year variation in planetary wave forcing (EXP3) produce lower stratospheric ozone responses between 0°–20°S that are larger than the response to solar UV variations alone (EXP1). The fact that the EXP3 lower stratospheric ozone response is larger than the EXP4 response indicates the importance of the QBO in producing a quasi-decadal signal in lower stratospheric ozone.

To provide a more quantitative assessment of the ozone response among the different experiments, Figure 18 compares the vertical profile of annual mean solar regression coefficients for ozone averaged between 0°–20°S from EXP1 (solid black curve), EXP2 (solid gray curve), EXP3 (dashed gray curve), and EXP 4 (dashed black curve) with the corresponding profile of SBUV(/2) regression coefficients and their 2σ uncertainty estimates for the 1979–2003 period [Soukharev and Hood, 2006]. Regression coefficients from EXP0 (black dotted curve), with no solar UV variation, are also plotted in Fig. 18 to quantify the quasi-decadal signal in low-latitude ozone produced by the interaction of the QBO with the annual cycle.

Comparison of the observed and modeled solar cycle ozone responses in Figure 18 shows that the combined effects of solar UV, the QBO, and planetary wave forcing in EXP3 produce a peak lower stratospheric ozone response of ∼2.5% between 22–24 km that is in good agreement with the observed lower stratospheric response at these latitudes. The EXP4 results show the largest ozone response in the upper stratosphere between 45–50 km.

None of the model experiments with imposed solar UV variations are able to reproduce the negligible response seen in SBUV(/2) ozone between 30–40 km, although it appears that dynamical variability related to the QBO and planetary wave forcing (i.e., results from EXP2 and EXP3 in Fig. 18) acts to reduce the 11-year ozone response to solar UV changes alone (EXP0) in this altitude region.

Figure 17 shows that the enhanced lower stratospheric ozone (and temperature) response in EXP3 can be associated with a decrease in the tropical upwelling at solar maximum (i.e., negative anomaly in $\bar{w}^*$) between 0°–20°S near 25 km. The reduced upwelling means there is less ozone-poor air transported up from lower altitudes and less adiabatic cooling in this region.

Figure 17 also shows that the larger upper stratospheric ozone response in both EXP3 and EXP4 is related to a positive anomaly in $\bar{w}^*$ at solar maximum over the equator near 50 km. This anomaly indicates increased upwelling and adiabatic cooling that acts to reduce the overall positive temperature response caused by increased ozone heating at solar maximum. As ozone is photochemically controlled in this region, the dynamically-induced reduction in temperature at solar maximum leads to more ozone due to the inverse relation between ozone and temperature in the upper stratosphere [Jucks and Salawitch, 2000]. This anomaly also explains the reduced upper stratospheric temperature response at low latitudes in EXP3 and EXP4 (Fig. 14 and 16, respectively) as compared to EXP2 (Fig. 10).

While the improved agreement between the modeled and observed 11-year ozone response shown in Figure 18 is encouraging, the overall vertical and meridional structure of the modeled ozone response still differs significantly from the SBUV(/2) response in

other areas, most notably with regard to the near zero ozone response that is observed near 35 km. Lee and Smith [2003] noted that this feature could be an artifact of volcanic effects in the observational record. Although our experiments do not include the impact of volcanic aerosols on ozone, we can conclude that dynamical variability related to the QBO and imposed changes in planetary wave 1 amplitude is not likely to reduce the "pure" ozone response to solar UV changes near 35 km by more than 0.5%.

6. Summary and Discussion

Results from a 150-year CHEM2D model simulation show that the average duration of the westerly QBO phase is 3 months shorter at solar maximum than at solar minimum. We find a similar effect in a 50-year model simulation that includes an imposed variation in planetary wave forcing in addition to the solar UV and QBO effects. These results confirm the initial findings of McCormack [2003] that the 11-year cycle in solar UV irradiance can influence the period of QBO in equatorial zonal winds. We find that the solar-QBO interaction is more robust in the present version of CHEM2D with higher vertical resolution compared to the McCormack [2003] results due to the reduced influence of the Rayleigh friction term. However, the modeled solar cycle modulation of the westerly QBO period is still smaller than the observed effect. Future studies should investigate whether or not additional feedback processes involving changes in parameterized equatorial wave dissipation due to ozone heating anomalies [Cordero and Nathan, 2005] are capable of amplifying the modeled solar-QBO interaction.

We also quantify the response of stratospheric ozone and temperature to changes in solar UV irradiance by applying a multiple linear regression model to 50 years of CHEM2D output. First, considering only solar UV variations, we reproduce the previously reported

discrepancies between the modeled and observed altitude dependence of the stratospheric ozone response. Specifically, the model ozone response peaks between 35–40 km, while the observed response exhibits two peaks in the upper stratosphere (40–50 km) and lower stratosphere (below 25 km) [e.g. Shindell et al., 1999; Hood, 2004]. Adding the effects of an interactive parameterization for the zonal wind QBO produces a modeled lower stratospheric ozone response of $\sim$2% that improves the agreement with the observed low latitude ozone response [Soukharev and Hood, 2006].

Including the effects of the QBO in the model produces a similar enhancement in the lower stratospheric temperature response of $\sim$0.4 K as well as enhanced zonal wind anomalies (i.e., solar maximum minus solar minimum) in the Northern winter extratropical stratosphere. Sorting these zonal wind anomalies according to the phase of the QBO shows that the poleward and downward propagation of westerly anomalies in the tropical upper stratosphere throughout the Northern winter during solar maximum is most pronounced during the QBO east phase. This result supports earlier observational studies that found a higher correlation between solar activity and polar stratospheric temperatures during QBO east years [e.g., Labitzke, 2005].

We also consider possible feedback between solar-induced changes in background zonal mean flow and planetary wave propagation in the winter extratropics by combining the effects of solar UV variations and the zonal wind QBO with an imposed 11-year variation in planetary wave 1 amplitude based on the observational estimates of Hood and Soukharev [2003]. The combination of smaller planetary wave forcing at solar maximum with the solar UV variations and the QBO produces further enhancement of the lower stratospheric ozone response. It also slightly reduces the ozone response between 30–

40 km and increases the ozone response between 45–55 km. This experiment produces the best overall agreement with the observed altitude dependence of the low-latitude ozone response (Fig. 5). The imposed planetary wave forcing does not improve the modeled ozone response in the absence of the QBO. One remaining discrepancy is that none of the experiments are able to reproduce the near zero ozone response found in the SBUV(/2) record between 30–40 km.

The improved agreement between the altitude dependence of the modeled and observed 11-year ozone response at low latitudes results from changes in stratospheric upwelling throughout the stratosphere (Fig 17). In the lower stratosphere, where ozone is controlled mainly by transport, reduced upwelling at low latitudes during solar maximum produces an enhancement in both ozone and temperature. In the upper stratosphere, where ozone is photochemically controlled, increased upwelling at low latitudes during solar maximum leads to a reduced positive temperature response (through adiabatic cooling) and thus an enhanced positive ozone response.

Although the 2D model experiments presented here do not exactly reproduce the altitude and latitude structure in the observed 11-year stratospheric ozone response, our findings indicate that a model with interactions between solar UV variations, the zonal wind QBO, and changes in planetary wave forcing of the middle atmosphere circulation can simulate key features of the SBUV(/2) ozone response that have been previously unexplained. It should be emphasized that, unlike 3D general circulation models, CHEM2D cannot simulate wave-mean flow interactions in a fully self-consistent manner. While the imposed 11-year variation in planetary wave 1 amplitude used in EXP3 and EXP4 is consistent with the hypothesis that changes in solar UV can produce a weaker planetary wave

forcing of the residual circulation at solar maximum, a non-solar origin for the planetary wave forcing is also possible.

Ultimately, a 3D modeling approach that includes an internally generated QBO and SAO in equatorial stratospheric zonal winds [e.g., Giorgetta et al., 2006] would be ideal for investigating possible dynamical feedbacks that can contribute to the 11-year ozone response. As the results of this study indicate, it is likely that current discrepancies between modeled and observed solar-cycle variations in stratospheric ozone can be reconciled as we improve our understanding of the decadal variability in stratospheric dynamics produced by coupling between the solar cycle, the QBO, and planetary wave activity.

Acknowledgments. The authors thank the reviewers for their constructive comments. We gratefully acknowledge B. Soukharev for assistance in providing the SBUV(/2) regression coefficients. This work was supported in part by the NASA Living with a Star TR&T program and by the Office of Naval Research.

References

Andrews, D. G., J. R. Holton and C. B. Leovy (1987), *Middle Atmosphere Dynamics*, Academic Press, 489 pp.

Austin, J., L. L. Hood, and B. E. Soukharev (2006), Solar cycle variations of stratospheric ozone and temperature in simulations of a coupled chemistry-climate model, *Atmos. Chem. Phys. Discuss., 6*, 12,121-12,153.

Baldwin, M. P., *et al.* (2001), The quasi-biennial oscillation, *Rev. Geophys., 39*, 179–229.

Brunner, D., J. Staehelin, J. A. Maeder, I. Wohltmann, and G. E. Bodeker (2006), Variability and trends in total and vertically resolved stratospheric ozone, *Atmos. Chem.*

Phys. Discuss., 6, 6317-6368.

Cordero, E. C., and T. R. Nathan (2005), A new pathway for communicating the 11-year solar cycle signal to the QBO, *Geophys. Res. Lett.,* 32, L18805, doi:10.1029/2005GL023696.

Crooks, S. A., and L. J. Gray (2005), Characterization of the 11-year solar signal using a multiple linear regression analysis of the ERA-40 dataset, *J. Climate, 18*, 996–1015.

Dunkerton, T. J. (1979), On the role of the Kelvin wave in the westerly phase of the semiannual zonal wind oscillation, *J. Atmo. Sci., 36*, 32–41.

Giorgetta, M. A., E. Manzini, Roeckner, E., Esch, M., and Bengston, L. (2006), Climatology and forcing of the quasi-biennial oscillation in the MAECHAM5 model., *J. Climate, 19*, 3882-3901, 2006.

Gray, L. J., and J. A. Pyle (1989), A two-dimensional model of the quasi-biennial oscillation of ozone, *J. Atmo. Sci, 46*, 203–220.

Gray, L. J., S. Crooks, C. Pascoe, S. Sparrow, M. Palmer (2004), Solar and QBO influences on the timing of stratospheric sudden warmings, *J. Atmos. Sci., 61*, 2777–2796.

Haigh, J.D. (1996), The impact of solar variability on climate, *Science, 272*, 981–984.

Hamilton, K. (2002), On the quasi-decadal modulation of the stratospheric QBO period, *J. Clim., 15*, 2562–2565.

Holton, J. R., and R. S. Lindzen (1972), An updated theory for the quasi-biennial cycle of the tropical stratosphere, *J. Atmo. Sci., 29*, 1076–1080.

Holton, J. R., and H. Tan (1980), The influence of the equatorial Quasi-Biennial Oscillation on the global circulation at 50 mb, *J. Atmos. Sci, 37*, 2200–2208.

Holton, J. R., P. H. Haynes, M. E. McIntyre, A. R. Douglass, R. B. Rood, and L. Pfister (1995), Stratosphere-troposphere exchange, *Rev. Geophys., 33,*, 403-439, 1995.

Hood, L. L. and J. P. McCormack (1992), Components of interannual ozone change based on Nimbus 7 TOMS data, *Geophys. Res. Lett., 19*, 23, 2309–2312.

Hood, L. L., J. L. Jirikowic, and J. P. McCormack (1993), Quasi-decadal variability of the stratosphere: Influence of long-term solar ultraviolet variations, *J. Atmos. Sci., 50*, 24, 3941-3958.

Hood, L. L. (1997), The solar cycle variation of total ozone: Dynamical forcing in the lower stratosphere, *J. Geophys. Res., 102*, D1, 1355–1370.

Hood, L. L., and B. E. Soukharev (2003), Quasi-decadal variability of the tropical lower stratosphere: The role of extratropical wave forcing, *J. Atmos. Sci., 60*, 2389–2403.

Hood, L. L. (2004), Effects of solar UV variability on the stratosphere, in *Solar Variability and its Effects on Climate*, Geophysical Monograph Series No. 141, J. Pap and P. Fox, eds., American Geophysical Union, Washington, DC, 366pp.

Hood, L. L., and B. E. Soukharev (2006), Solar induced variations of odd nitrogen: Multiple regression analysis of UARS HALOE data, *Geophys. Res. Lett., in press.*

Jucks, K. W., and R. J. Salawitch (2000), Future changes in upper stratospheric ozone, in Atmospheric Science Across the Stratopause, Geophysical Monograph Series no. 123, D. E. Siskind, S. D. Eckermann, and M. E. Summers, eds., American Geophysical Union, Washington DC, 342 pp.

Kodera, K. J. P. McCormack, and M. Giorgetta (1997), Influence of the solar cycle on climate through stratospheric processes, in *The Stratosphere and its Role in Climate System, NATO Advanced Study Institute Series I: Global Environmental Change, Vol.*

54, G. Brasseur, ed., 365pp., Springer-Verlag, New York.

Kodera, K., and Y. Kuroda (2002), Dynamical response to the solar cycle, *J. Geophys. Res., 107* (D24), 4749, doi:10.1029/2002JD002224.

Kuroda, Y., and K. Kodera (2002), Effect of solar activity on the polar-night jet oscillation in the Northern and Southern Hemisphere winter, *J. Meteorol. Soc. Japan, 80*, 4B, 973–984.

Labitzke, K., and H. van Loon (1988), Associations between the 11-year solar cycle, the QBO, and the atmosphere. Part I: the troposphere and stratosphere in the northern hemisphere winter, *J. Atmos. Terr. Phys.,* 50, 3, 197–206.

Labitzke, K., (2005), On the solar cycle-QBO relationship: A summary, *J. Atmos. Sol.-Terr. Phys., 67*, 45–54.

Langematz, U., J. L. Grenfell, K. Matthes, P. Mieth, M. Kunze, B. Steil, C. Brül (2005), Chemical effects in 11-year solar cycle simulation with the Freie Universität Berlin Climate Middle Atmosphere Model with online chemistry (FUB-CMAM-CHEM), *Geophys. Res. Lett., 32*, L13803, doi:10.1029/2005GL022686.

Lean, J. L., et al. (1997), Detection and parameterization of variations in solar mid- and near-ultraviolet radiation (200-400 nm), *J. Geophys. Res., 102*, 29,939–29,956.

Lee, H., and A. K. Smith (2003), Simulation of the combined effects of solar cycle, quasi-biennial oscillation, and volcanic forcing on stratospheric ozone changes in recent decades, *J. Geophys. Res., 108*(D2), 4049, doi:10.1029/2001JD001503.

Matthes, K., U. Langematz, L. J. Gray, K. Kodera, and K. Labitzke (2004) Improved 11-year solar signal in the Freie Universität Berlin Climate Middle Atmosphere Model (FUB-CMAM), *J. Geophys. Res., 109*, D06101, doi:10.1029/2003JD004012.

Matthes, K., Y. Kuroda, K. Kodera, U. Langematz (2006), Transfer of the solar signal from the stratosphere to the troposphere: Northern winter, *J. Geophys. Res., 111*, D06108, doi:10.1029/2005JD006283.

McCormack, J. P., and L. L. Hood (1996), Apparent solar cycle variations of upper stratospheric O_3 and temperature: Latitude and seasonal dependences, *J. Geophys. Res., 101*, 20,933–20,944.

McCormack, J. P., L. L. Hood, R. Nagatani, A. J. Miller, W. G. Planet, and R.D. McPeters (1997), Approximate separation of volcanic and 11-year signals in the SBUV-SBUV/2 total ozone record over the 1979-1995 period, *Geophys. Res. Lett., 24*, 22, 2729–2732.

McCormack, J. P., and D. E. Siskind (2002), Simulations of the quasi-biennial oscillation and its effect on stratospheric H_2O, CH_4, and age of air with an interactive two-dimensional model, *J. Geophys. Res., 107* (D22), 4625, doi:10.1029/2002JD002141.

McCormack, J. P. (2003), The influence of the 11-year solar cycle on the quasi-biennial oscillation, *Geophys. Res. Lett., 30*(22), 2162, doi:10.1029/2003GL018314.

McCormack, J. P., S. D. Eckermann, D. E. Siskind, and T. J. McGee (2006), CHEM2D-OPP: A new linearized gas-phase ozone photochemistry parameterization for high-altitude NWP and climate models, *Atmos. Chem. Phys., 6*, 4943–4972.

Palmer, M. A., and L. J. Gray (2005), Modeling the atmospheric response to solar irradiance changes using a GCM with a realistic QBO, *Geophys. Res. Lett., 32*, L24701, doi:10.1029/2005GL023809.

Pascoe, C. L., L. J. Gray, S. A. Crooks, M. N. Juckes, and M. P. Baldwin (2005), The quasi-biennial oscillation: Analysis using ERA-40 data, *J. Geophys. Res., 110*, D08105, doi:10.1029/2004JD004941.

Quiroz, R. S. (1981), Period modulation of the stratospheric quasi-biennial oscillation, *Mon. Wea. Rev., 109*, 665–674.

Randel, W. J., and J., and J. B. Cobb (1994), Coherent variations of monthly mean column ozone and lower stratospheric temperature, *J. Geophys. Res., 99* (D3), 5433-5447.

Randel, W. J., and F. Wu (1996), Isolation of the ozone QBO in SAGE II data by singular value decomposition, *J. Atmos. Sci., 53*, 2546-2559.

Rind, D. (2002), The sun's role in climate variations, *Science, 296*, 673–677.

Salby, M., and P. Callaghan (2000), Connection between the solar cycle and the QBO: The missing link?, *J. Clim., 13*, 2652–2662.

Salby, M. L., and P. F. Callaghan (2006), Relationship of the quasi-biennial oscillation to the stratospheric signature of the solar cycle, *J. Geophys. Res., 111*, D06110, doi:10.1029/2005JD006012.

Sander, S.P., et al. (2003), Chemical kinetics and photochemical data for use in atmospheric studies, Evaluation No. 14, Jet Propulsion Laboratory, Pasadena CA, USA.

Shindell, D., D. Rind, N. Balachandran, J. Lean, and P. Lonergan (1999), Solar cycle variability, ozone, and climate, *Science, 284*, 305–308.

Siskind, D. E. (2000), On the coupling between middle and upper atmospheric odd nitrogen, in Atmospheric Science Across the Stratopause, Geophysical Monograph Series no. 123, D. E. Siskind, S. D. Eckermann, and M. E. Summers, eds., American Geophysical Union, Washington DC, 342 pp.

Siskind, D. E., S. D. Eckermann, J. P. McCormack, M. J. Alexander, and J. T. Bacmeister (2003), Hemispheric differences in the temperature of the summertime stratosphere and mesosphere, *J. Geophys. Res., 108* (D2), 4051, doi:10.1029/2002JD002095.

Stratospheric Processes and Their Role in Climate (SPARC)(1998), *Assessment of trends in the vertical distribution of ozone, World Meteorological Organization - Ozone Research and Monitoring Project Rep. No. 43*, N. Harris, R. Hudson, and C. Phillips, eds.

Soukharev, B. E., and L. L. Hood (2006), The solar cycle variation of stratospheric ozone: Multiple linear regression analysis of long-term satellite data sets and comparisons with models, *J. Geophys. Res., in press.*

World Meteorological Organization (1991), *Scientific Assessment of Ozone Depletion: 1991, Global Ozone Research and Monitoring Project – Rep. No. 25*, WMO Ozone Secretariat, Geneva.

World Meteorological Organization (2003), *Scientific Assessment of Ozone Depletion: 2002, Global Ozone Research and Monitoring Project–Report No. 47*, WMO Ozone Secretariat, Geneva.

Table 1. Description of experiments

Experiment	Description
EXP0	Fixed solar UV with zonal wind QBO
EXP1	Varying solar UV without zonal wind QBO
EXP1RF	Same as EXP1 using McCormack [2003] Rayleigh friction profile
EXP2	Varying solar UV with zonal wind QBO
EXP3	Varying solar UV with zonal wind QBO and planetary wave forcing
EXP4	Varying solar UV with planetary wave forcing and without QBO

Figure 1. (a) Altitude/time section of CHEM2D equatorial zonal wind from the control experiment (EXP0), westerly winds are shaded, contours are drawn for 0, ±10, ±20, ±40, and ±60 m s^{-1}. (b) Vertical profiles of annual mean CHEM2D equatorial zonal wind (solid curve) and climatological values obtained from the UARS Reference Atmosphere Project (dashed curve).

Figure 2. The standardized time series representing solar UV variations and the first two principal components of the zonal wind QBO used in the multiple linear regression model.

Figure 3. Spatial patterns of the ozone regression coefficients (a) γ_{QBO1} and (b) γ_{QBO2}, associated with the first and second principal components of the CHEM2D equatorial stratospheric zonal wind respectively, from the control experiment (EXP0). Coefficients are expressed as the percent change for a one standard deviation change in the principal component time series. Shaded regions are not statistically significant at the 2σ level.

Figure 4. Annual average ozone solar regression coefficients, expressed as the percent change (solar maximum minus solar minimum) from Experiment 1, which includes an imposed 11-year cycle in solar UV. Solid contours denote positive values, dashed contours denote negative values, shaded areas are not significant at the 2σ level. Contours are drawn every $\pm 0.5\%$ up to $\pm 4\%$, and then every $\pm 2\%$ thereafter.

Figure 5. Annual average ozone solar regression coefficients derived from the combined SBUV(/2) ozone profile data set for the period 1979-2003. [Soukharev and Hood, 2006]. Regression coefficients are expressed as the percentage difference between solar maximum and solar minimum. Shaded regions are not statistically significant at the 2σ level.

Figure 6. (a) Profiles of the Rayleigh friction time scales in Experiment 1 (black curve) and Experiment 1RF (gray curve). Experiment 1RF is identical to the profile used in McCormack [2003]. (b) Solar-induced anomalies in the equatorial zonal wind at 50 km from Experiment 1 (black curve) and Experiment 1RF (gray curve). Dashed vertical line indicates solar maximum.

Figure 7. (a) Time series of CHEM2D equatorial zonal winds at 32 hPa from Experiment 1 with fixed solar UV (black curve) and Experiment 2 with varying solar UV (gray curve). Dashed vertical lines indicate solar maximum.

Figure 8. Lengths of individual easterly (E) and westerly (W) model zonal wind QBO phases at 32 hPa, sorted according to the phase of the solar cycle, from Experiment 2. The solar irradiance intervals are defined to be within ±20 months of the maximum or minimum in UV irradiance.

Figure 9. Annual average solar regression coefficients for ozone (percentage change, solar maximum minus solar minimum) from Experiment 2, which includes both solar UV and QBO effects. Shaded regions are not statistically significant at the 2σ level.

Figure 10. Annual average solar regression coefficients for temperature, expressed as the change (Kelvin) between solar maximum and solar minimum, from Experiment 2 that includes both solar UV and QBO effects. Shaded regions are not statistically significant at the 2σ level.

Figure 11. Composite zonal wind differences (in m s^{-1}, solar maximum minus solar minimum) computed on the first day of December, January, and February from (a) EXP1 with solar cycle and no QBO, (b) EXP2 with solar cycle and QBO, (c) EXP2 for QBO east years only, and (d) EXP2 for QBO west years only. Contours are drawn every ±1,±2,±4,±6,...,. Dashed contours indicate negative values. Light and dark gray shading denotes statistical significance at the 90% and 95% confidence levels, respectively.

Figure 12. (a) Latitude profile of planetary wave 1 amplitude imposed at the model lower boundary for conditions at solar maximum (dashed line) and solar minimum (solid line) in Experiment 3. (b) Time series of the vertical component of the Eliassen-Palm flux at 100 hPa for January, averaged between 30°–90°N latitude, from Experiment 3.

Figure 13. Annual average solar regression coefficients for ozone (percentage change between solar maximum and solar minimum) from Experiment 3, which includes varying solar UV, the QBO, and an imposed 11-year variation in planetary wave 1 amplitude. Shaded regions are not statistically significant at the 2σ level.

Figure 14. Annual average solar regression coefficients for temperature (change in Kelvin between solar maximum and solar minimum) from Experiment 3, which includes varying solar UV, the QBO, and an imposed 11-year variation in planetary wave 1 amplitude. Shaded regions are not statistically significant at the 2σ level.

Figure 15. Annual average solar regression coefficients for ozone (percentage change between solar maximum and solar minimum) from Experiment 4, which includes varying solar UV and an imposed 11-year variation in planetary wave 1 amplitude. Shaded regions are not statistically significant at the 2σ level.

Figure 16. Annual average solar regression coefficients for temperature (change in Kelvin between solar maximum and solar minimum) from Experiment 4, which includes varying solar UV and an imposed 11-year variation in planetary wave 1 amplitude. Shaded regions are not statistically significant at the 2σ level.

Figure 17. Annual mean composite differences in model vertical velocity $\bar{w}^*$ (mm $\sec^{-1}\times 10$), solar maximum minus solar minimum, from (a) EXP1, (b) EXP2, (c) EXP3, and (d) EXP4. The zero contour is solid, positive contours are dotted, and negative contours are dashed. The ± 0.1 contours are omitted above 45 km. Light and dark gray shading indicates regions where differences are statistically significant at the 90% and 95% confidence levels, respectively.

Figure 18. Annual mean solar regression coefficients from model experiments 0–4 averaged between 0° - 20°S, and corresponding solar regression coefficients (diamonds) derived from the 1979-2003 SBUV(/2) record with $\pm 2\sigma$ uncertainty estimates [Soukharev and Hood, 2006].

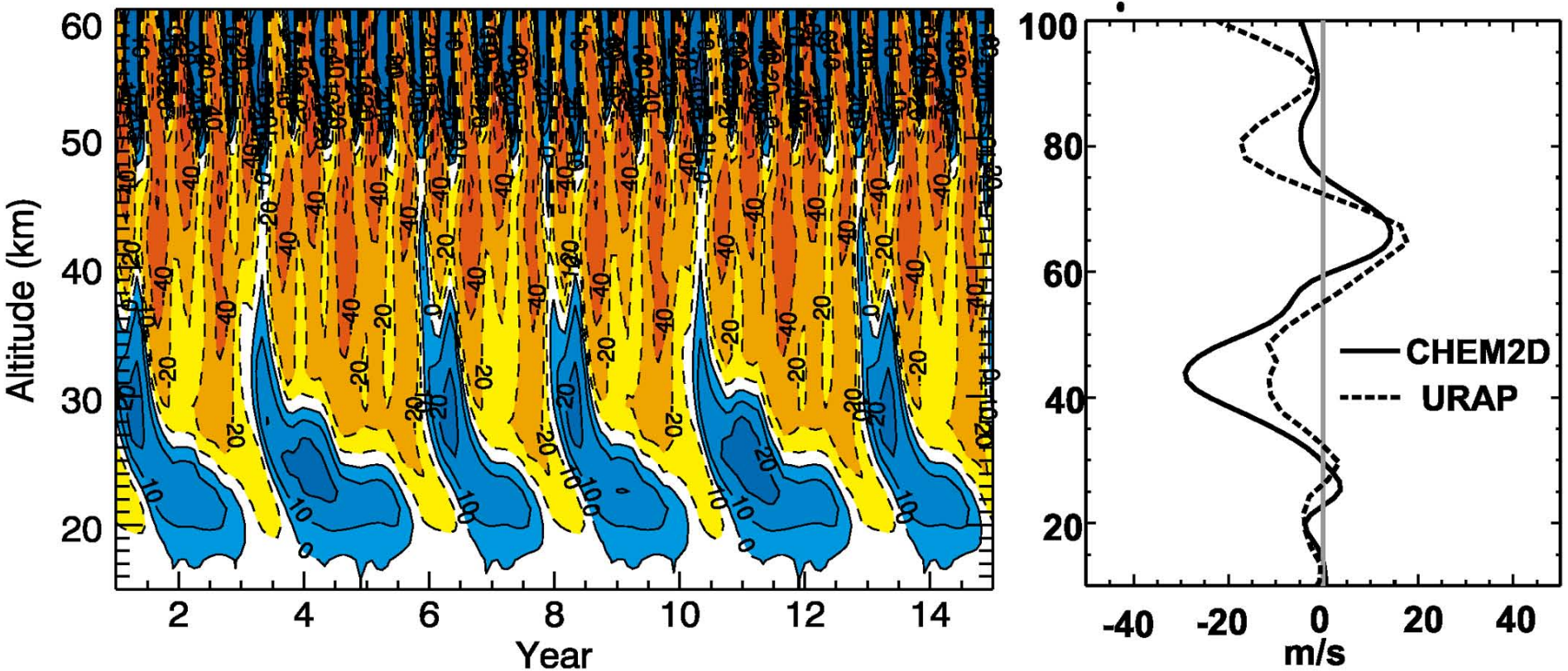
Altitude (km)
60
50
40
30
20
2
4
6
8
10
12
14
Year
100
80
60
40
20
CHEM2D
URAP
-40
-20
0
20
40
m/s

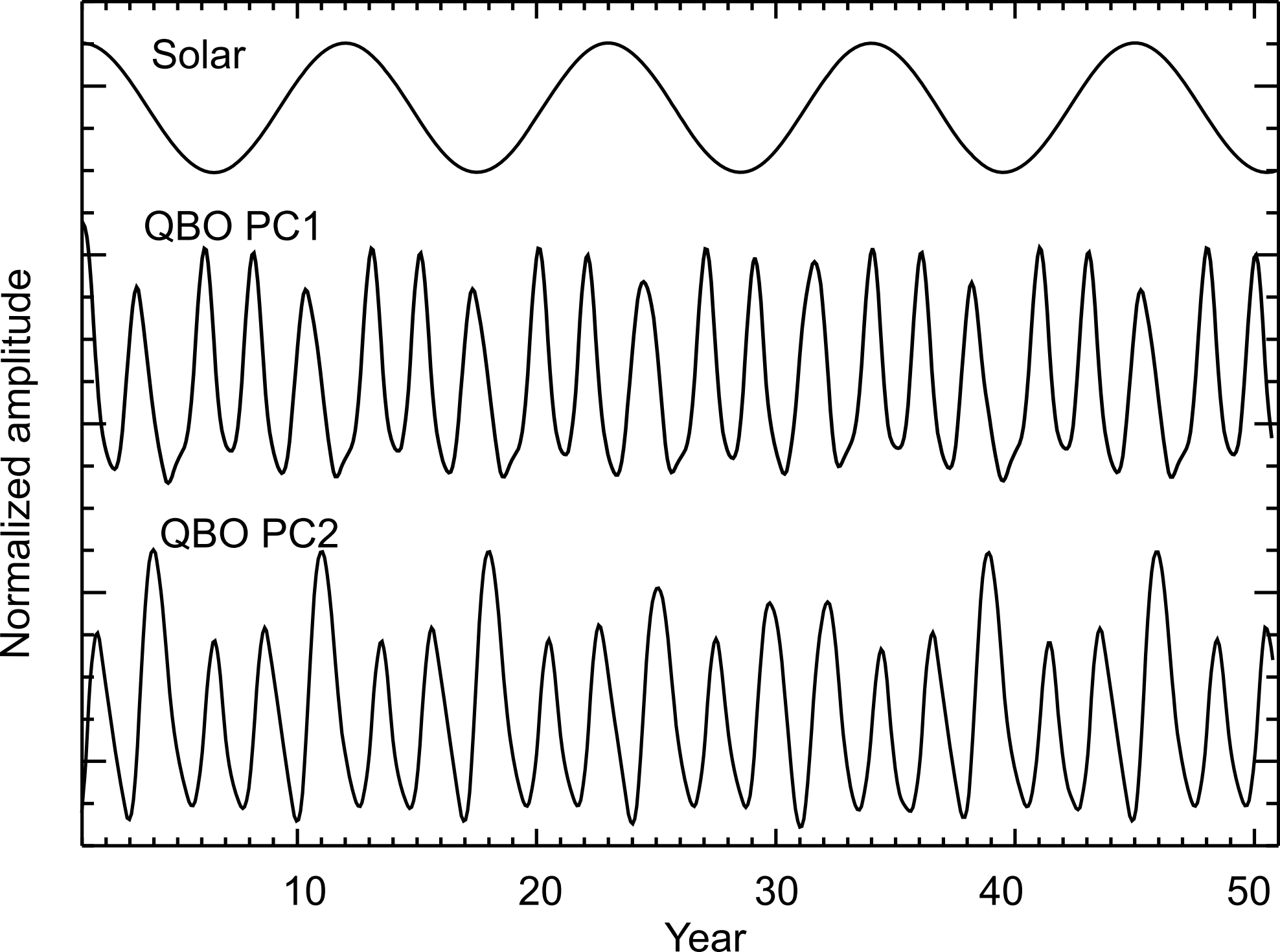
Solar
QBO PC1
QBO PC2
Normalized amplitude
10
20
30
40
50
Year

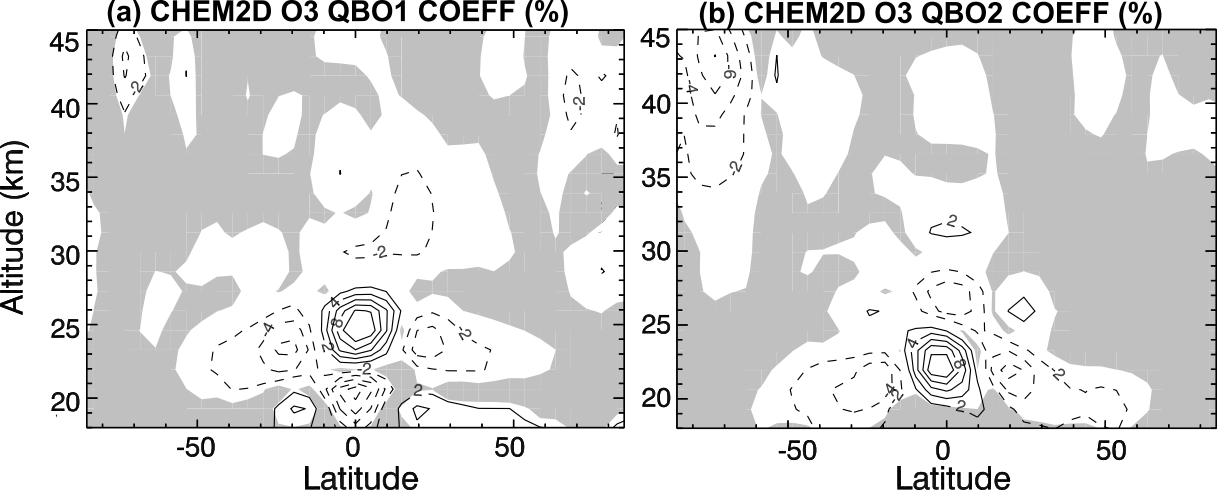
(a) CHEM2D O3 QBO1 COEFF (%)
(b) CHEM2D O3 QBO2 COEFF (%)
Altitude (km)
45
40
35
30
25
20
-50
0
50
Latitude
-50
0
50
Latitude

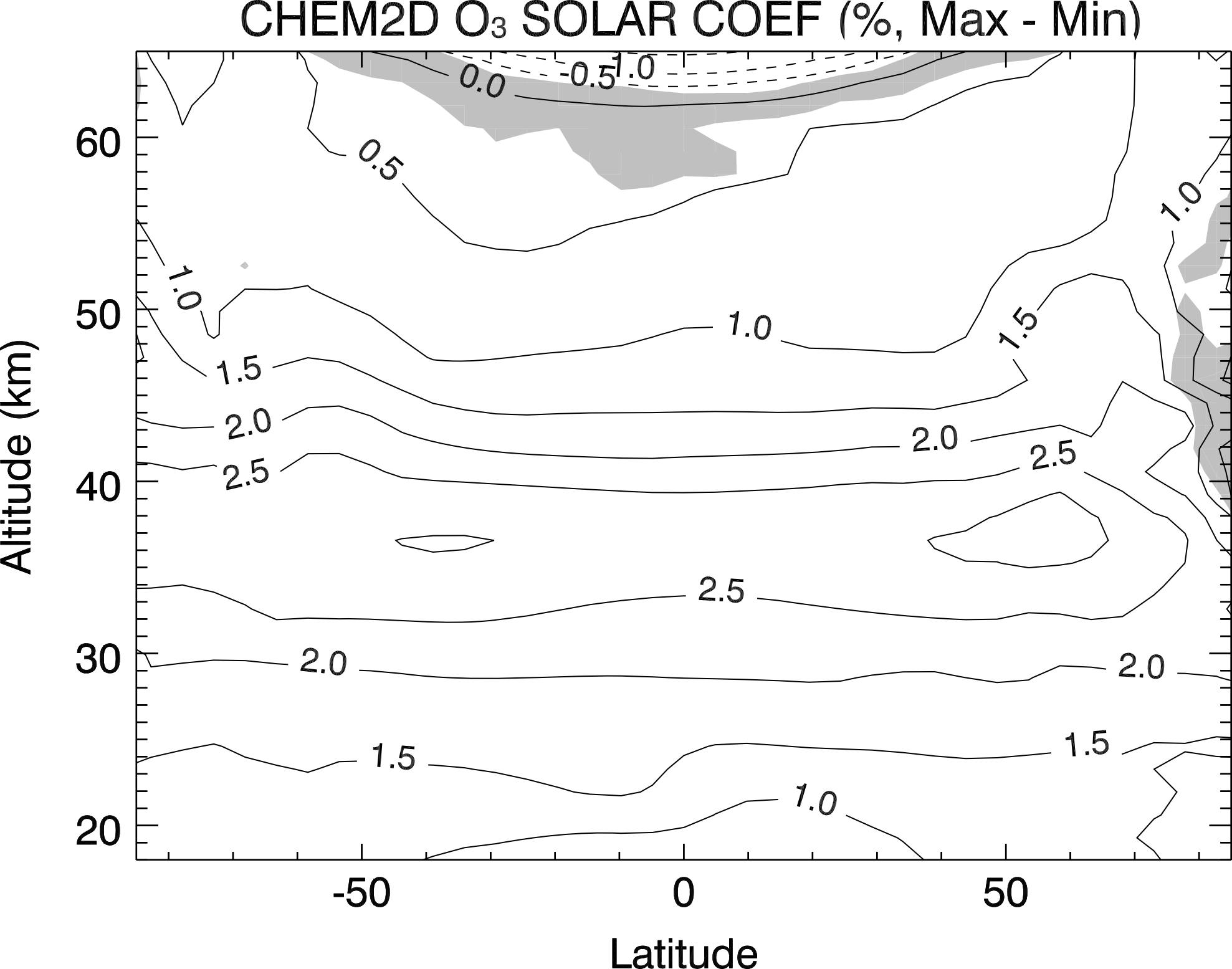
CHEM2D O3 SOLAR COEF (%, Max - Min)
Altitude (km)
Latitude
60
50
40
30
20
-50
0
50
0.0
-0.5
1.0
0.5
1.0
1.0
1.5
1.0
1.5
2.0
2.0
2.5
2.5
2.5
2.0
2.0
1.5
1.5
1.0

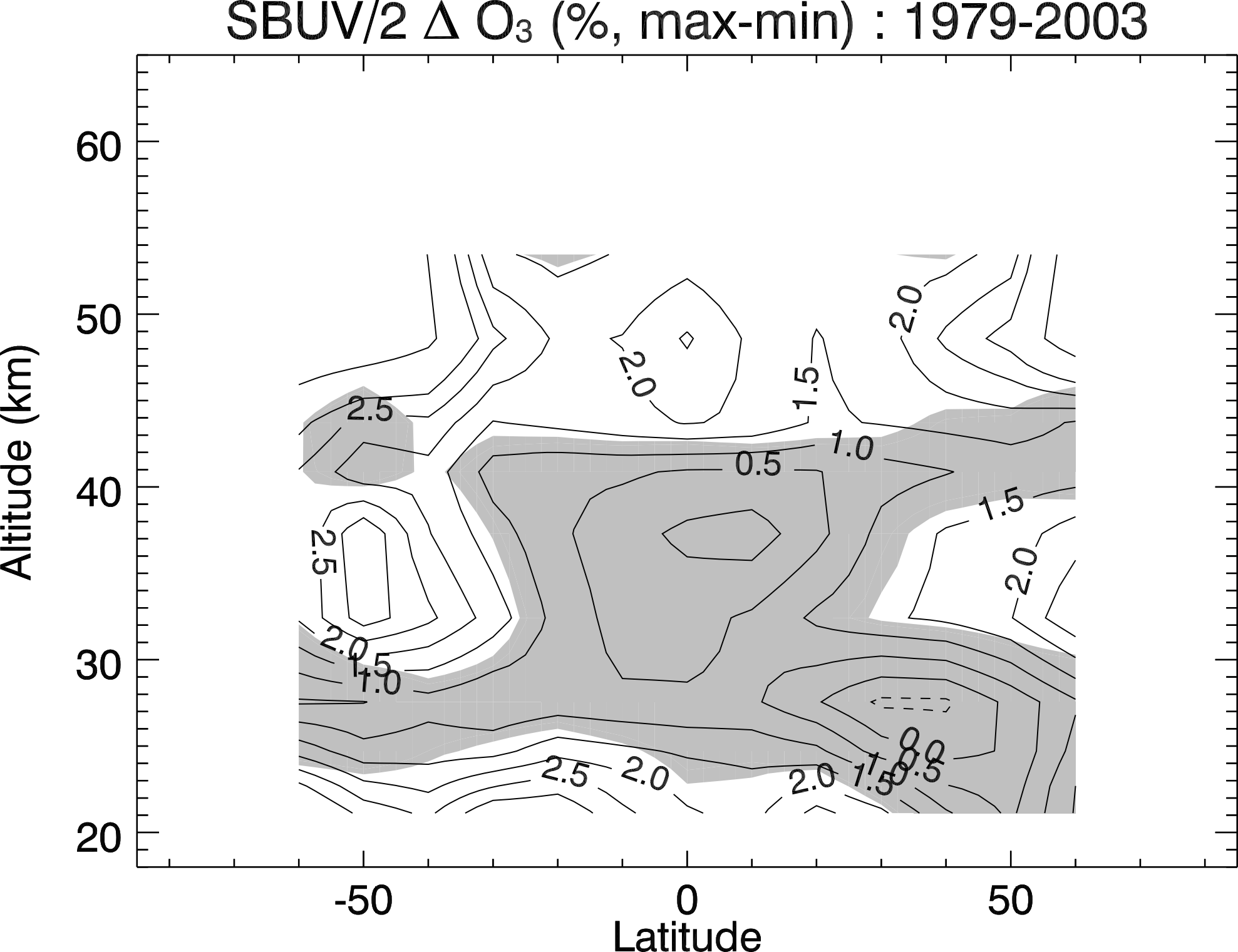
SBUV/2 Δ O3 (%, max-min) : 1979-2003
Altitude (km)
60
50
40
30
20
-50
0
50
Latitude
2.5
2.0
1.5
1.0
0.5
0.0

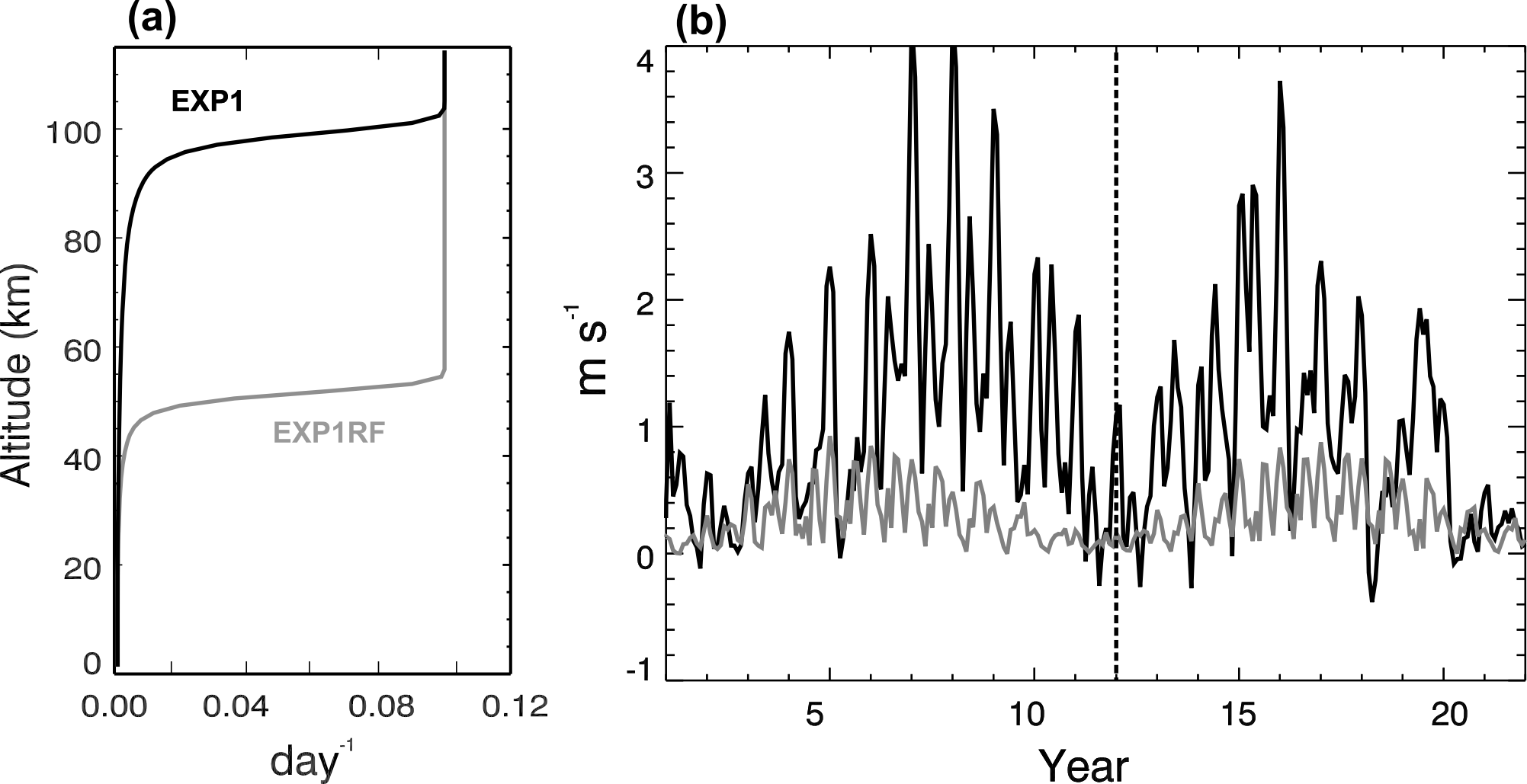
(a)
EXP1
EXP1RF
Altitude (km)
0
20
40
60
80
100
0.00
0.04
0.08
0.12
day-1
(b)
m s-1
-1
0
1
2
3
4
5
10
15
20
Year

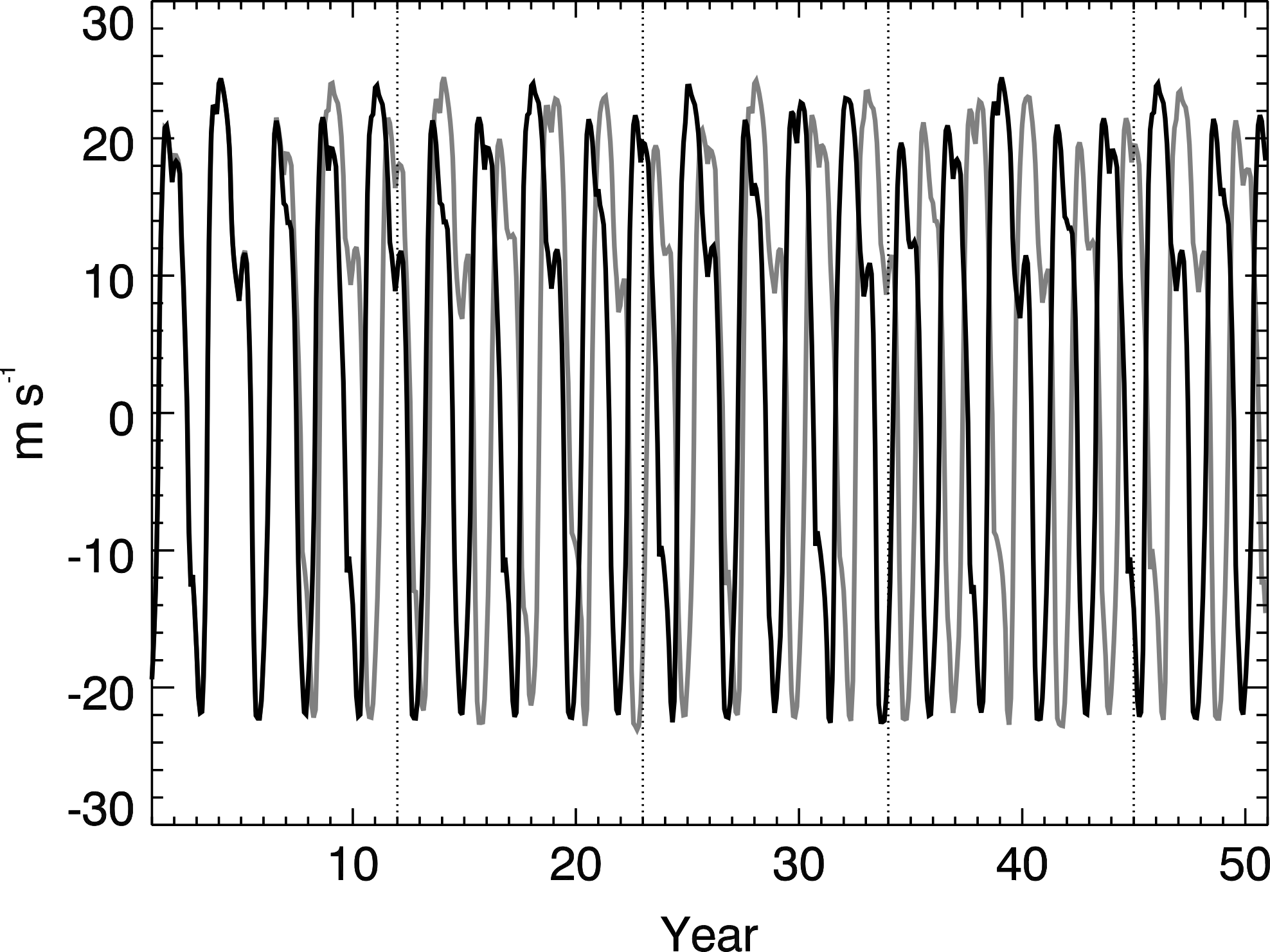
30
20
10
0
-10
-20
-30
m s-1
10
20
30
40
50
Year

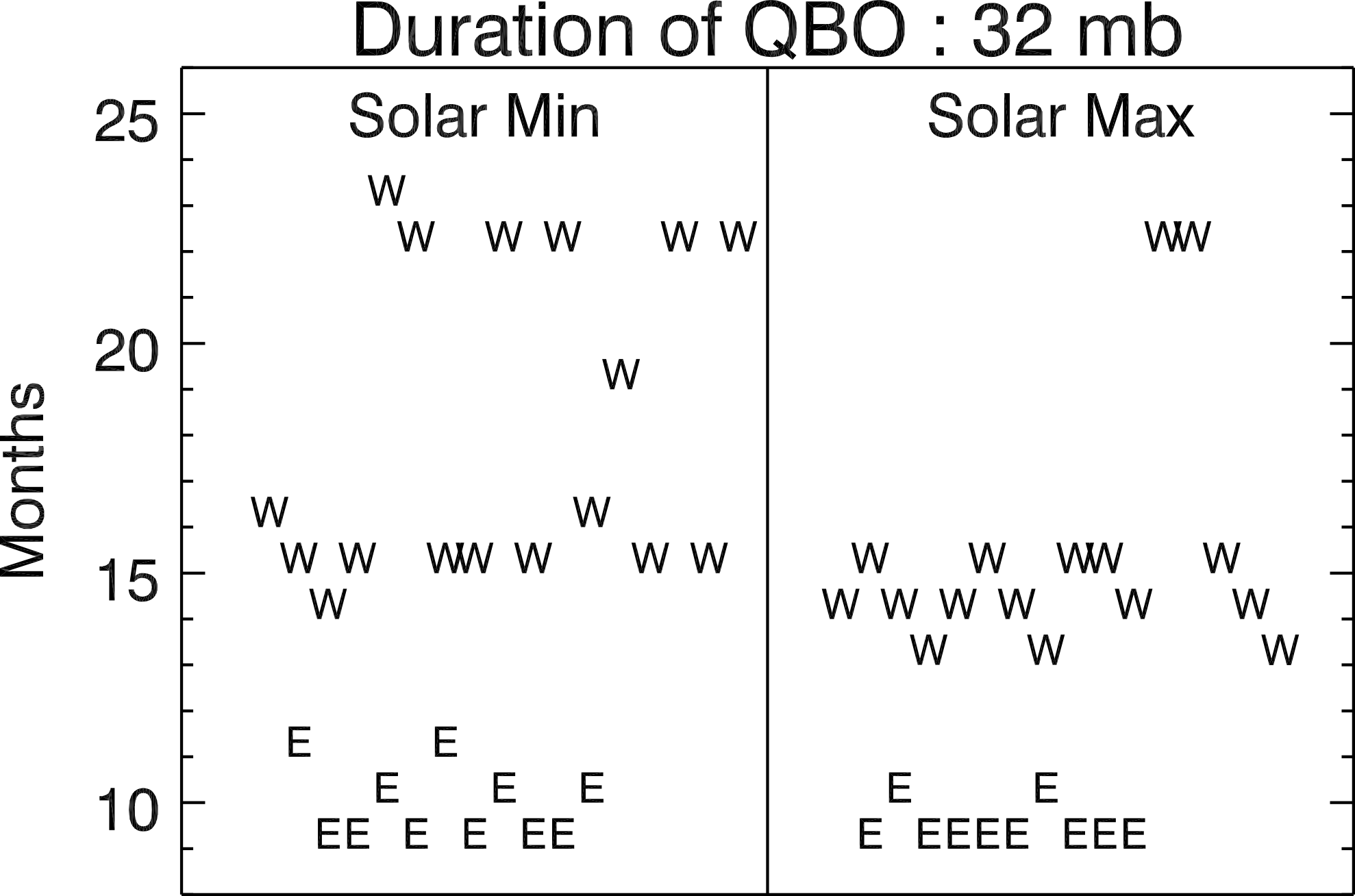
Duration of QBO : 32 mb
Solar Min
Solar Max
Months
25
20
15
10

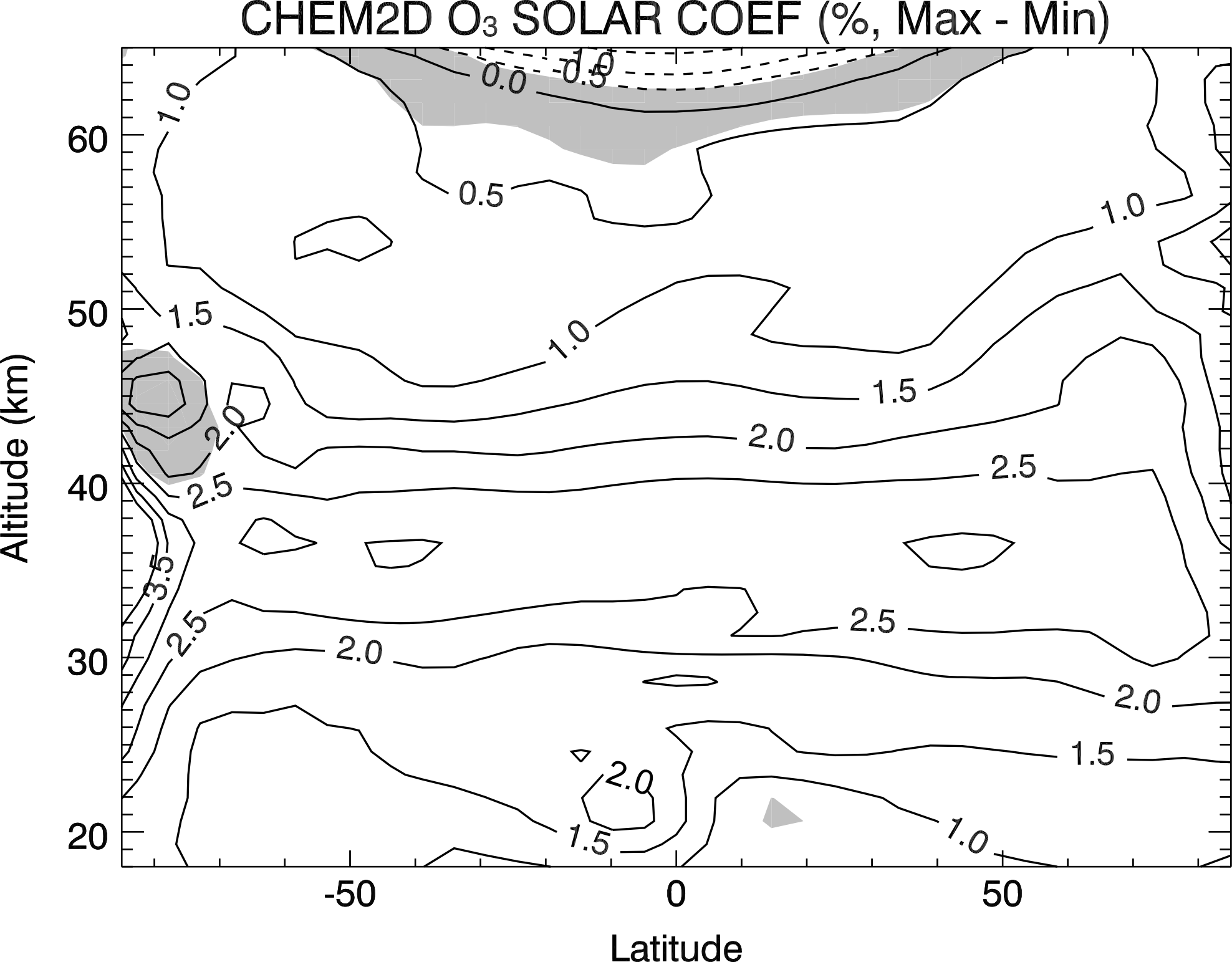
CHEM2D O3 SOLAR COEF (%, Max - Min)
Altitude (km)
Latitude
60
50
40
30
20
-50
0
50
1.0
0.0
0.5
0.5
1.0
1.5
1.0
1.5
2.0
2.0
2.5
3.5
2.5
2.5
2.0
2.0
2.0
1.5
1.5
1.0

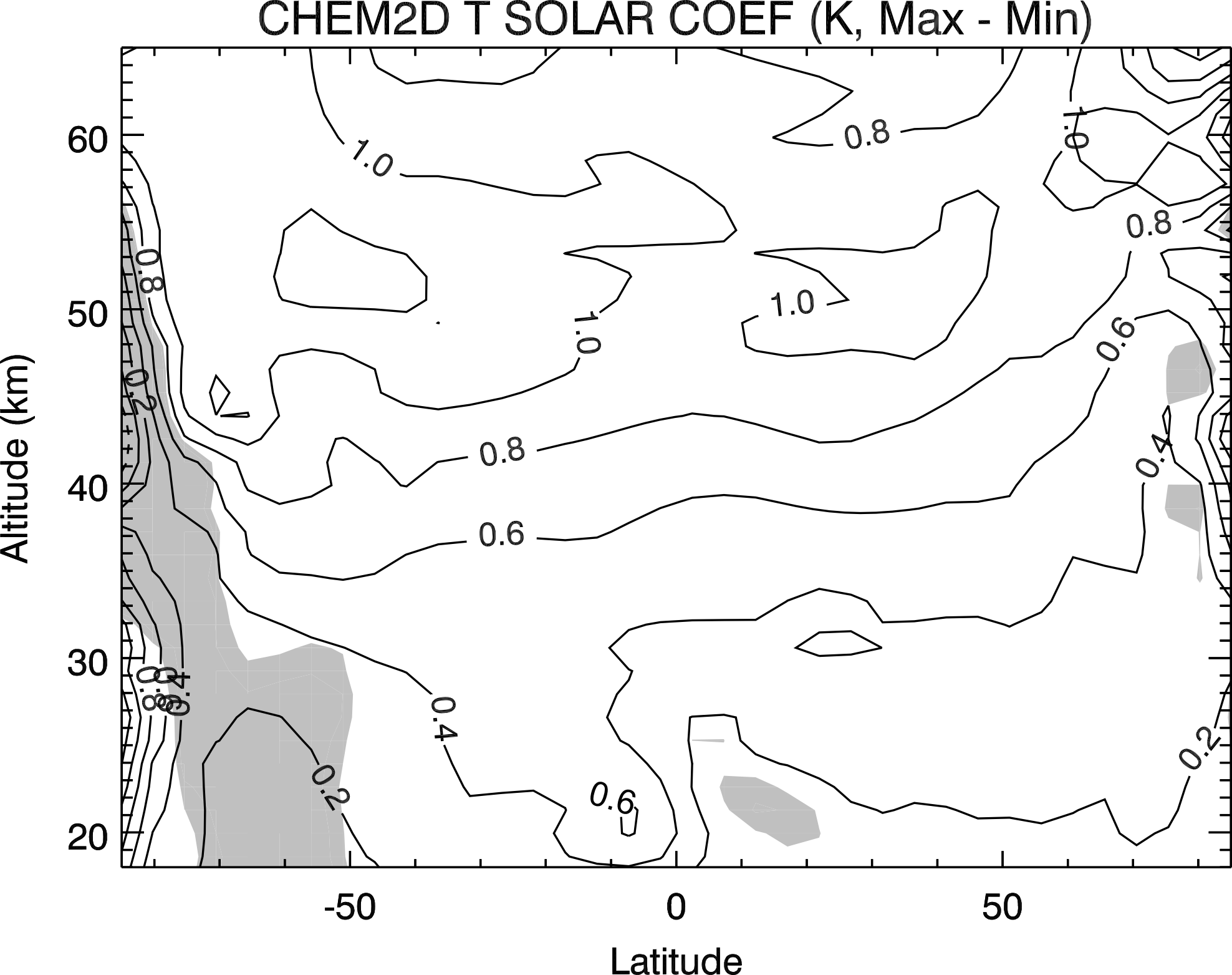
CHEM2D T SOLAR COEF (K, Max - Min)
Altitude (km)
60
50
40
30
20
-50
0
50
Latitude
1.0
0.8
0.6
0.4
0.2

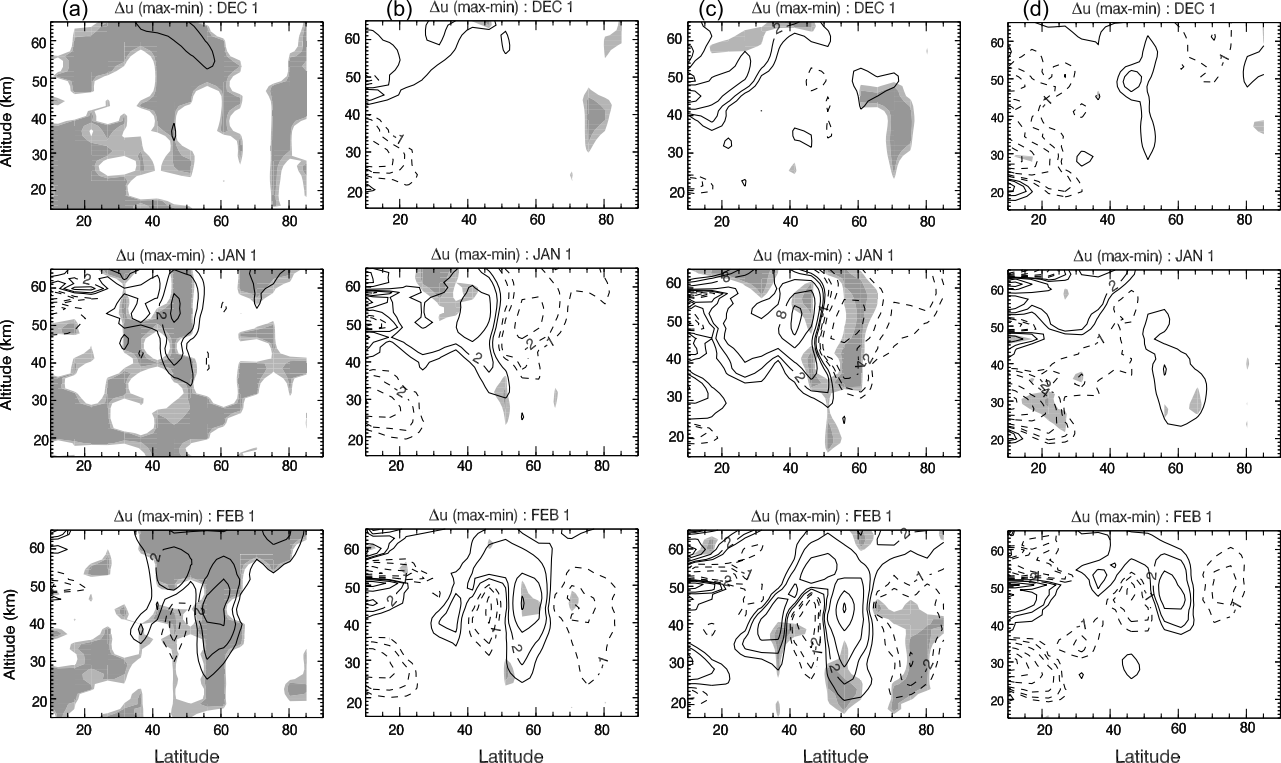
(a)
Δu (max-min) : DEC 1
(b)
Δu (max-min) : DEC 1
(c)
Δu (max-min) : DEC 1
(d)
Δu (max-min) : DEC 1
Δu (max-min) : JAN 1
Δu (max-min) : JAN 1
Δu (max-min) : JAN 1
Δu (max-min) : JAN 1
Δu (max-min) : FEB 1
Δu (max-min) : FEB 1
Δu (max-min) : FEB 1
Δu (max-min) : FEB 1
Altitude (km)
Latitude
20
30
40
50
60
20
40
60
80

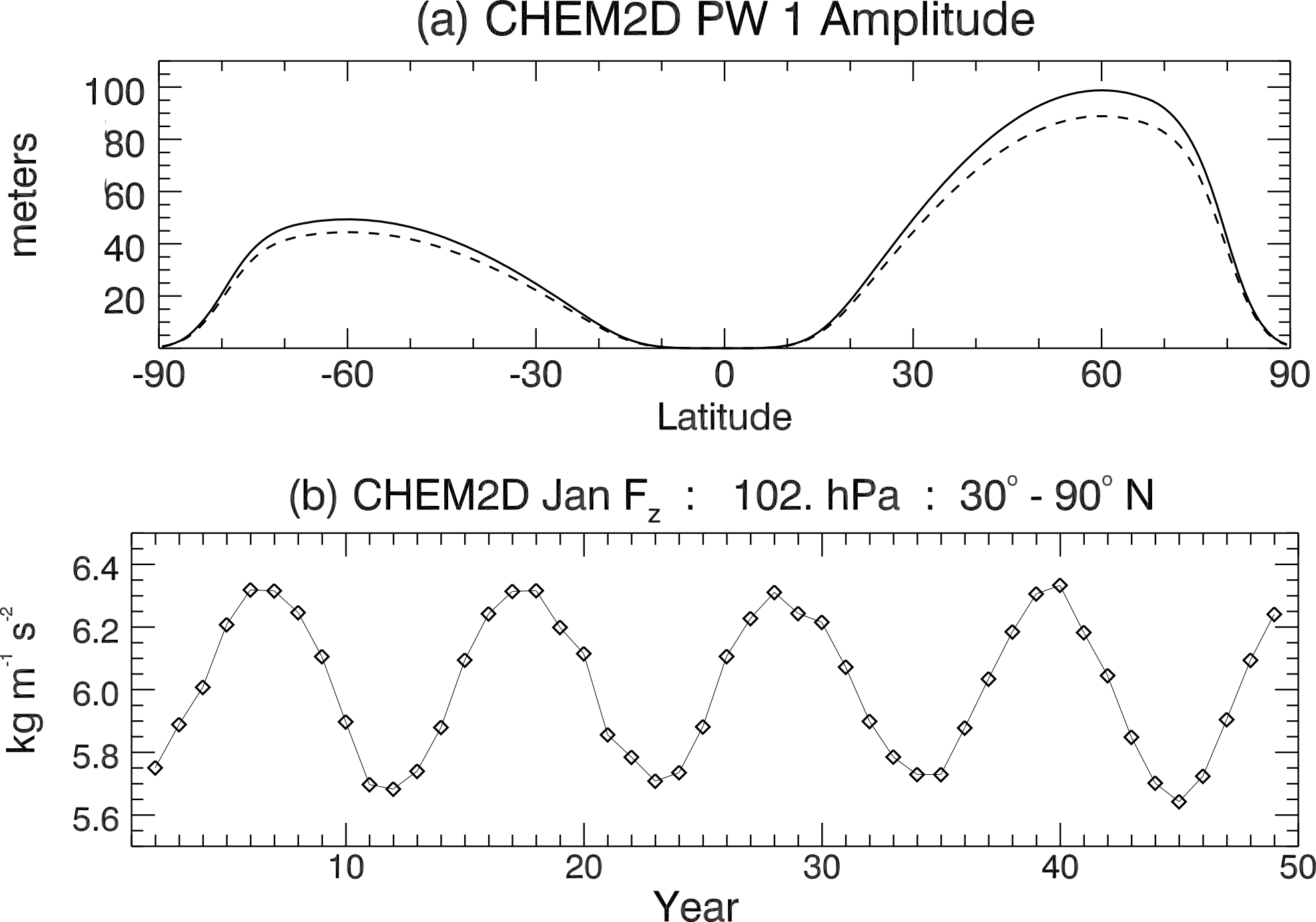
(a) CHEM2D PW 1 Amplitude
meters
100
80
60
40
20
-90
-60
-30
0
30
60
90
Latitude
(b) CHEM2D Jan F_z : 102. hPa : 30° - 90° N
kg m^{-1} s^{-2}
6.4
6.2
6.0
5.8
5.6
10
20
30
40
50
Year

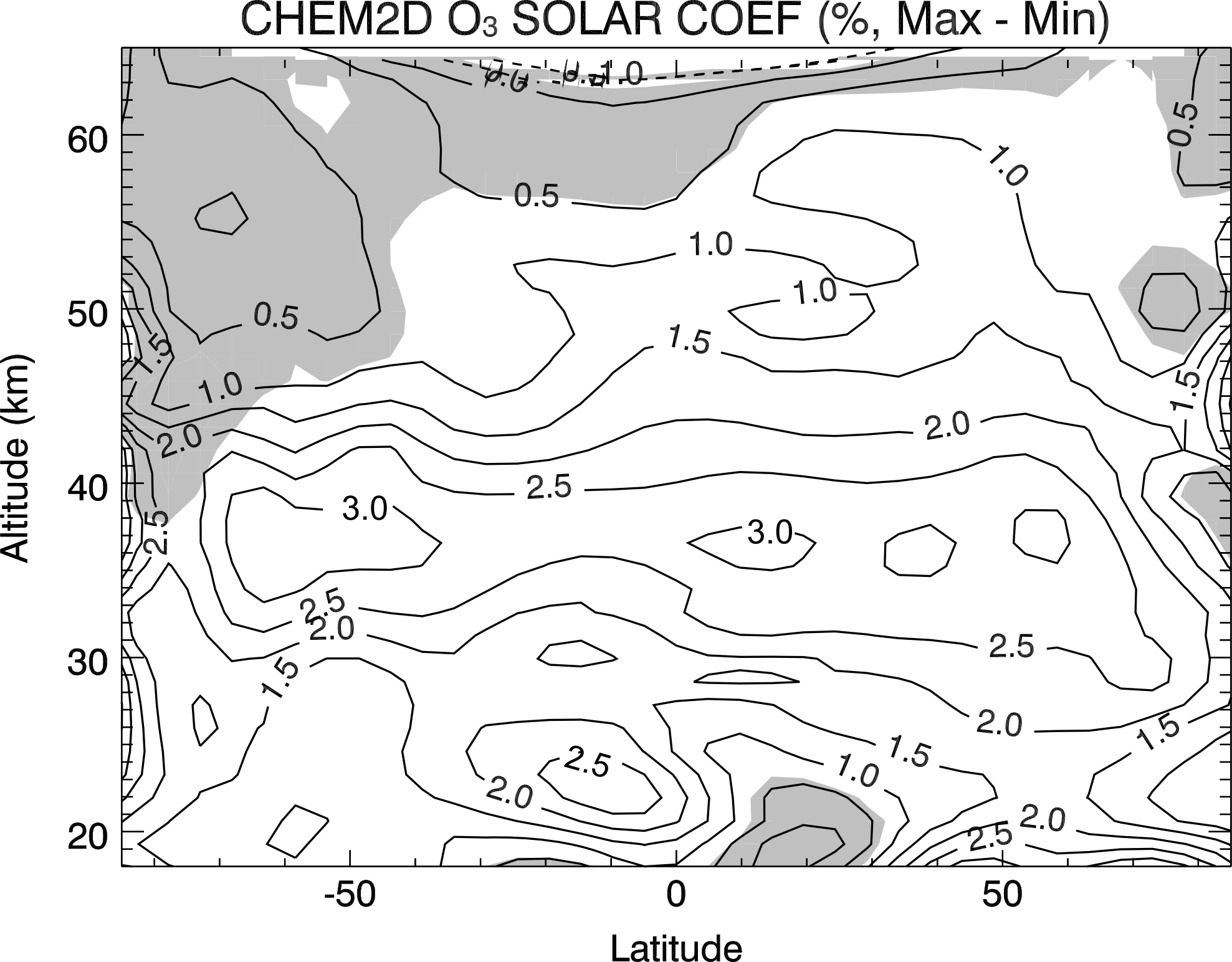
CHEM2D O3 SOLAR COEF (%, Max - Min)
Altitude (km)
Latitude
60
50
40
30
20
-50
0
50
0.5
1.0
1.5
2.0
2.5
3.0

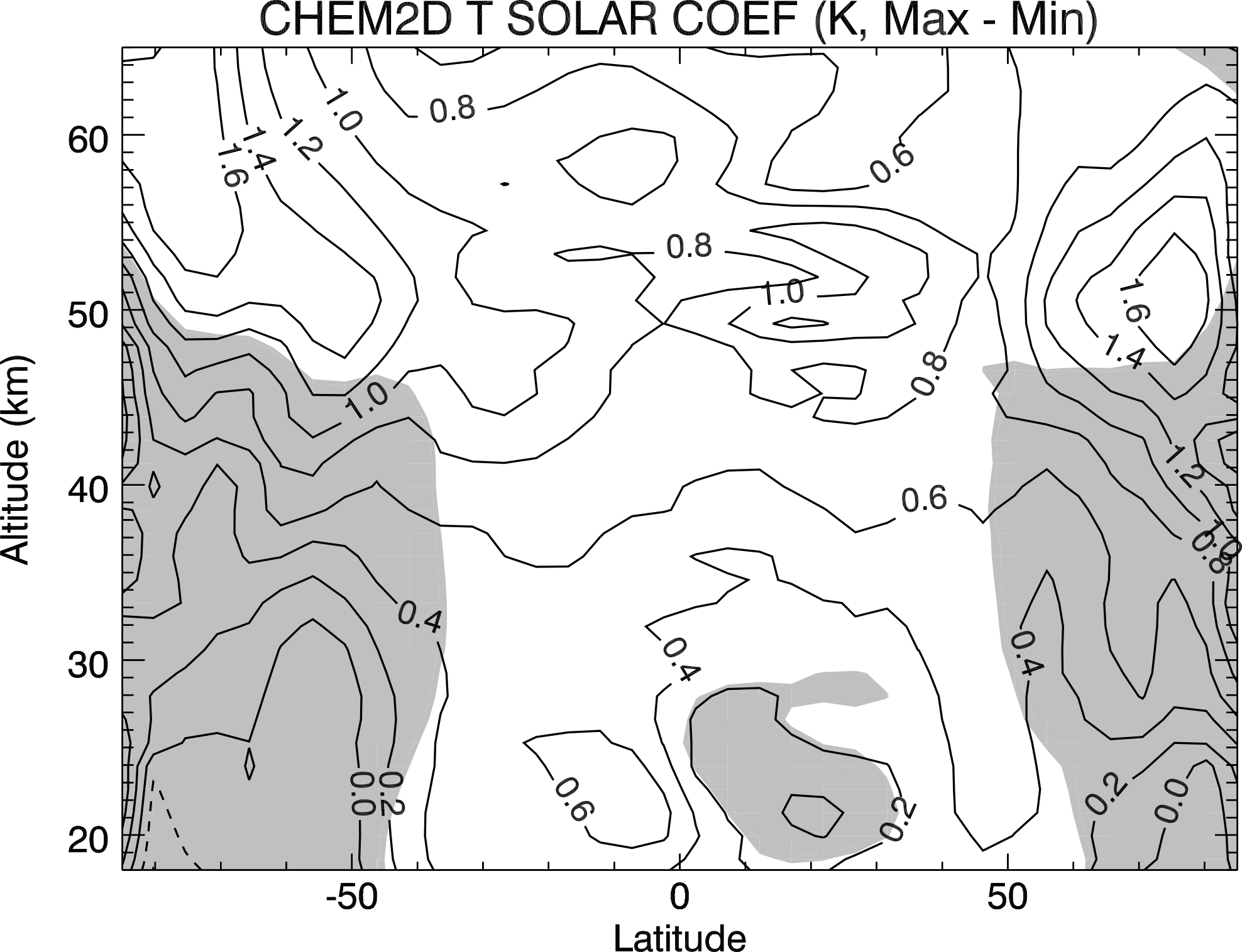
CHEM2D T SOLAR COEF (K, Max - Min)
Altitude (km)
60
50
40
30
20
-50
0
50
Latitude
1.6
1.4
1.2
1.0
0.8
0.6
0.4
0.2
0.0

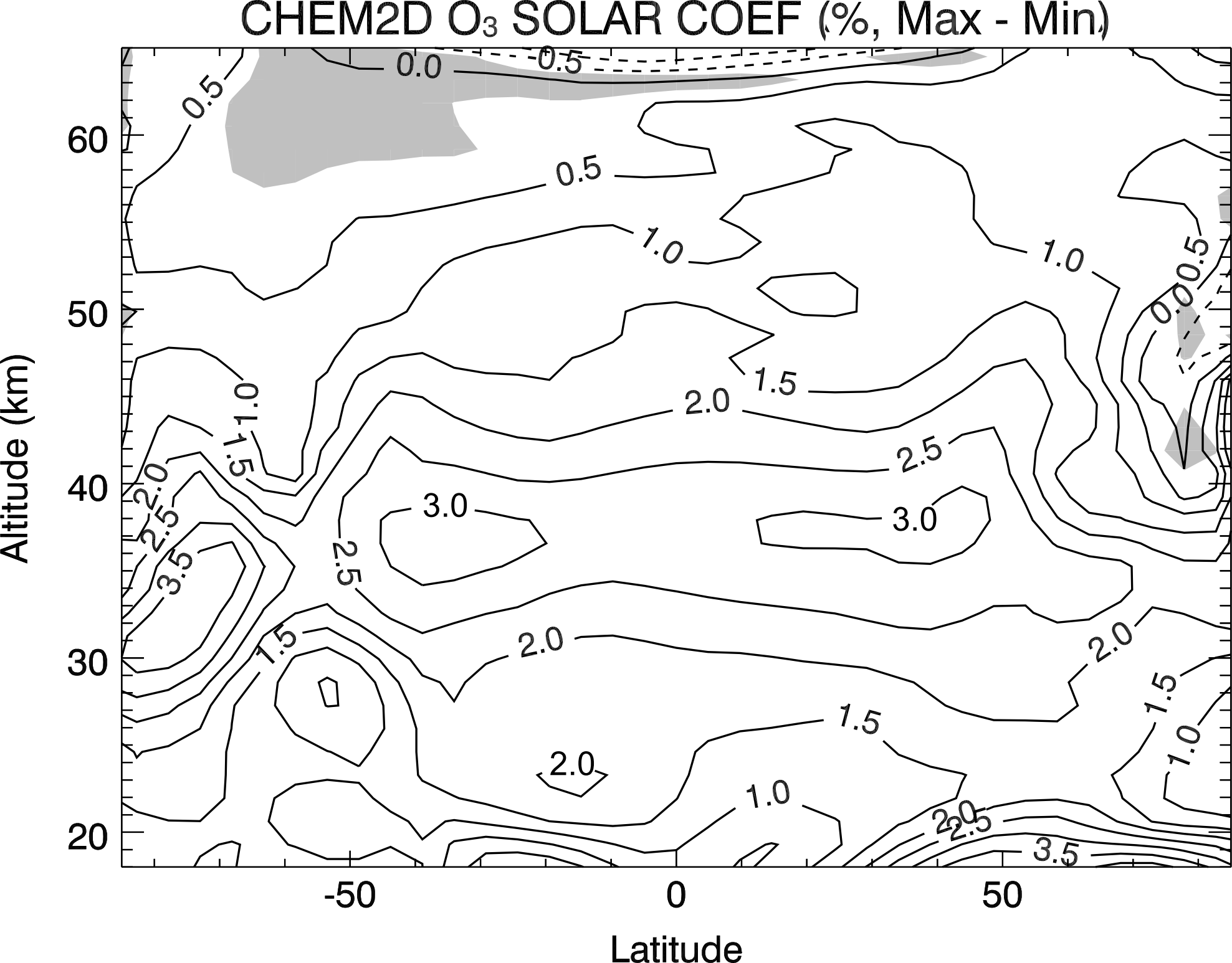
CHEM2D O3 SOLAR COEF (%, Max - Min)
Altitude (km)
Latitude
60
50
40
30
20
-50
0
50
0.0
0.5
1.0
1.5
2.0
2.5
3.0
3.5

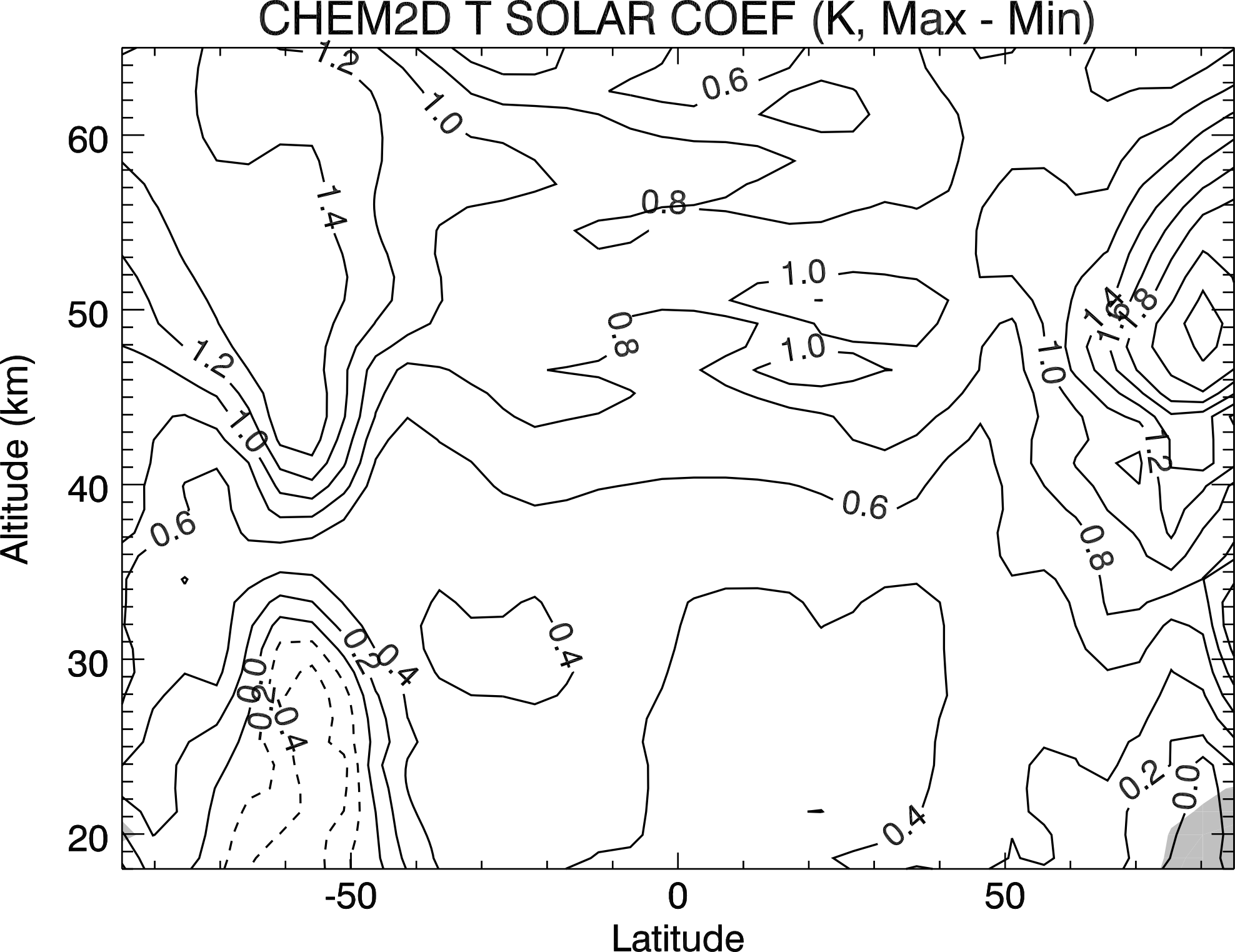
CHEM2D T SOLAR COEF (K, Max - Min)
Altitude (km)
60
50
40
30
20
-50
0
50
Latitude
1.2
1.0
0.6
1.4
0.8
1.0
0.8
1.0
1.2
1.0
0.6
1.0
1.4
1.8
1.2
0.6
0.8
0.4
0.2
0.4
0.0
-0.2
-0.4
0.2
0.0
0.4

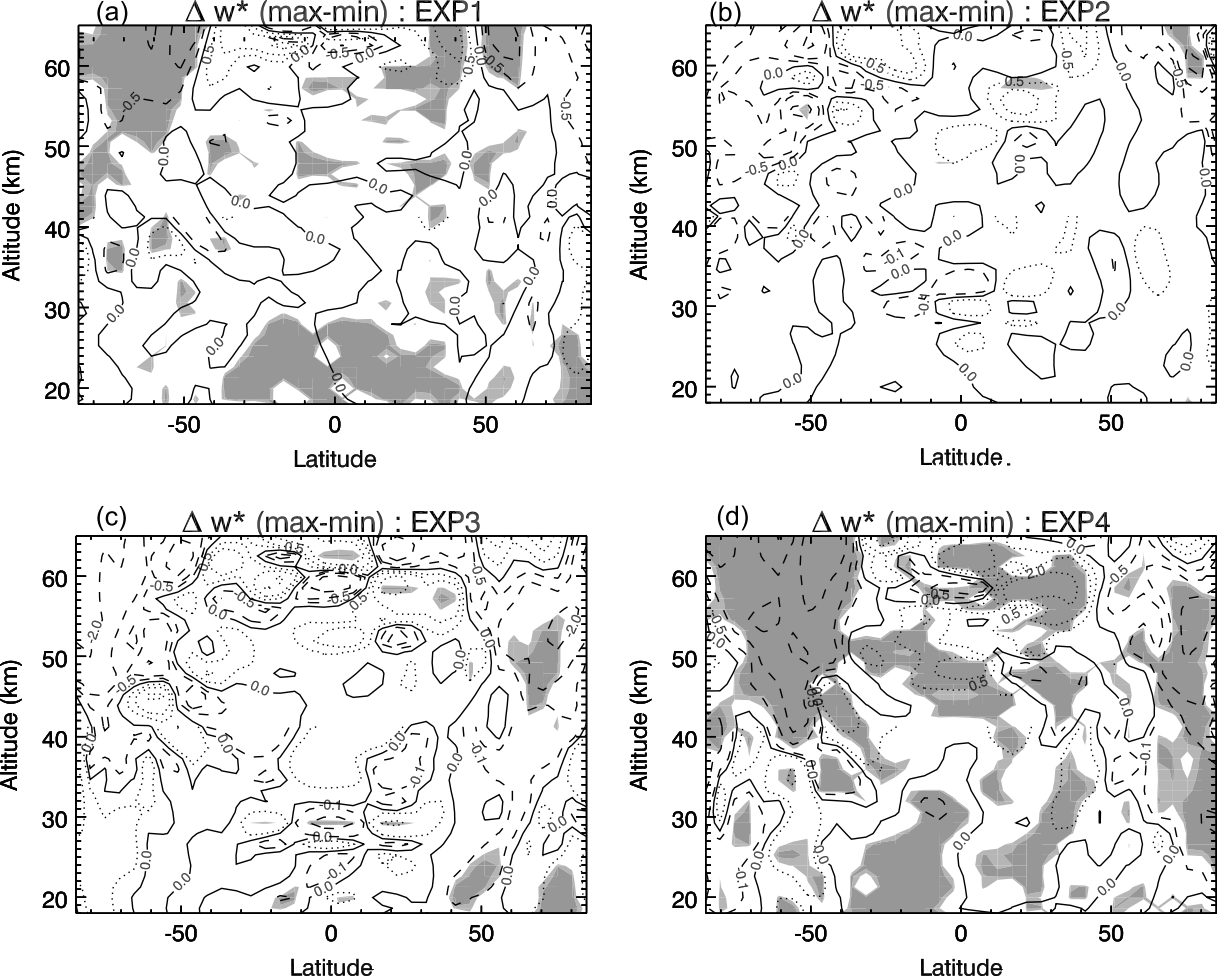
(a) Δ w* (max-min) : EXP1
(b) Δ w* (max-min) : EXP2
(c) Δ w* (max-min) : EXP3
(d) Δ w* (max-min) : EXP4
Altitude (km)
Latitude
20
30
40
50
60
-50
0
50

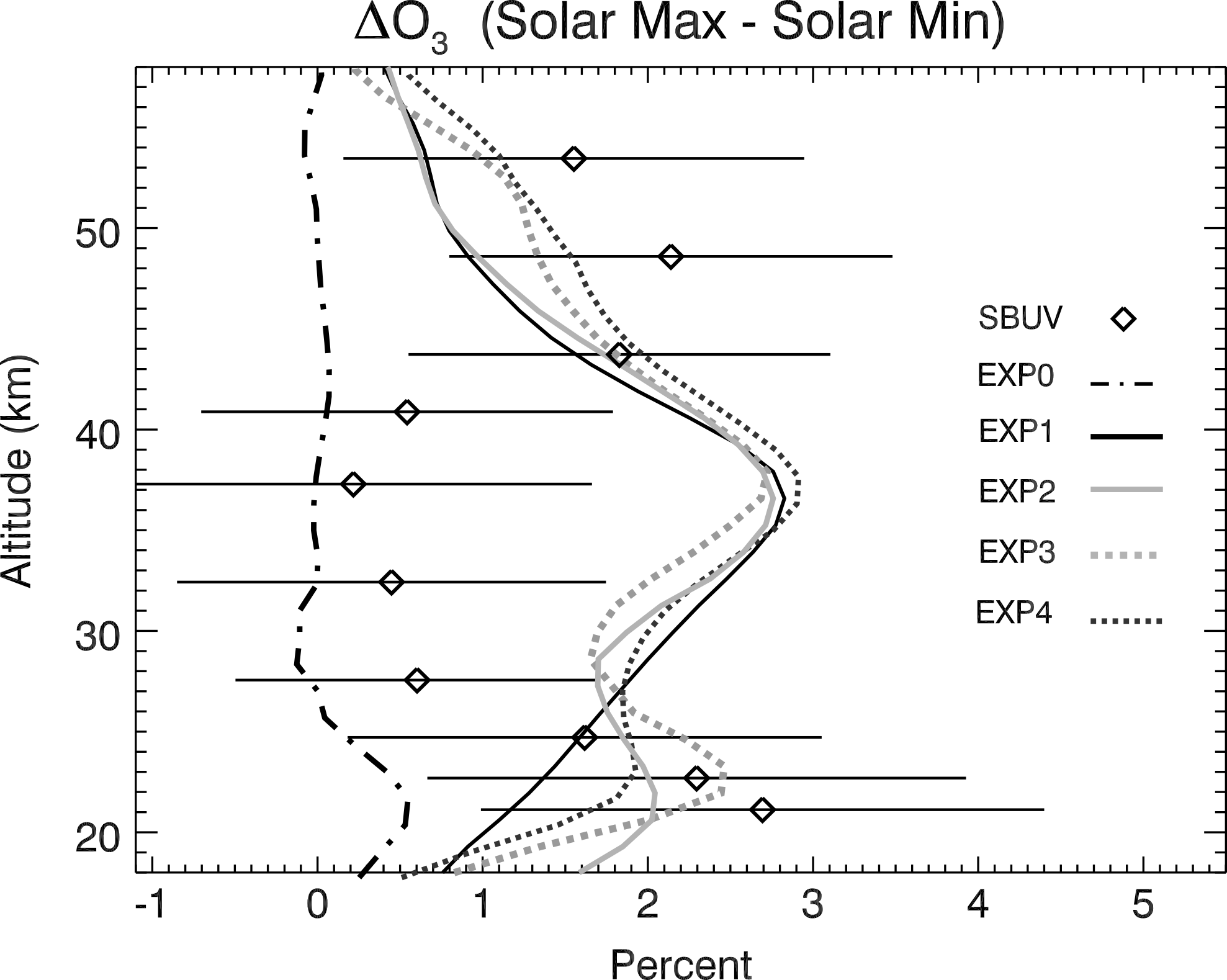
ΔO3 (Solar Max - Solar Min)
Altitude (km)
50
40
30
20
-1
0
1
2
3
4
5
Percent
SBUV
EXP0
EXP1
EXP2
EXP3
EXP4